Title
TRANSITION METAL OXIDE COATED TITANIUM ELECTRODES FOR REDOX BATTERIES

Author
Savinell, R.F.

Publication Date
1982-12-01

LBL-15716
UC-94cb

Lawrence Berkeley Laboratory
UNIVERSITY OF CALIFORNIA

ENERGY & ENVIRONMENT DIVISION

TRANSITION METAL OXIDE COATED TITANIUM ELECTRODES FOR REDOX BATTERIES

Robert F. Savinell

December 1982

ENERGY AND ENVIRONMENT DIVISION

Prepared for the U.S. Department of Energy under Contract DE-AC03-76SF00098

DISCLAIMER

TRANSITION METAL OXIDE COATED TITANIUM ELECTRODES FOR REDOX BATTERIES

Robert F. Savinell
Department of Chemical Engineering
The University of Akron
Akron, Ohio 44325

Final Report
to

Energy and Environment Division
Lawrence Berkeley Laboratory
University of California
Berkeley, California 94720

This work was supported by the Assistant Secretary for Conservation and Renewable Energy, Office of Energy Systems Research, Division of Energy Storage, U.S. Department of Energy under Contract No. DE-AC03-76SF00098.

TRANSITION METAL OXIDE COATED TITANIUM ELECTRODES FOR REDOX BATTERIES

Final Report

Robert F. Savinell
Department of Chemical Engineering
The University of Akron
Akron, Ohio 44325

University of California Subcontract No. 4512510
Contract Duration: April 15, 1982 - September 30, 1982
Contract Amount: $31,220

SUMMARY

The objective of this research program was to ascertain electrocatalytic activity of transition metal oxides for use as long life redox battery electrodes. A primary motivation for this work was to produce porous electrodes (of titanium) with reproducible surface activity for experiments to corroborate predictions of porous electrode theory. An additional goal of this research program was to ascertain if simple one-step outer-sphere electron transfer mechanism applies to the ferric-ferrous redox reaction at high reactant/product concentrations in a strong acid chloride medium. Kinetic rate expressions of this couple under these conditions at the metal oxide surfaces were sought.

Coatings of the conductive and active rutile structure form of selected transition metal oxides (namely RuO_2, IrO_2, OsO_2) were desired. Both IrO_2 and RuO_2 coatings having the rutile structure (as confirmed by x-ray diffraction) were prepared by thermal decomposition of their respective hydrated chloride salts. In the case of OsO_2 only amorphous coatings have been achieved. Failure to obtain the rutile structure is apparently due to the conversion of OsO_2 to the volatile OsO_4 at baking temperatures. Further work with OsO_2 was not pursued.

The determination of the electrochemically active surface area is important in evaluating the intrinsic activity of electrode materials. Since variations in the coating techniques and in substrate condition along with handling and electrochemical history all markedly effect the true surface area, a measurement of the actual surface area of the RDE is required immediately prior to taking kinetic measurements. The voltammetric charge (0.05 to 1.0 V vs SCE, 20 mV/s, in 1 M H_2SO_4 at 25°C) was used as a means of estimating the disk surface area. The correlation of charge with true surface area (as measured by Zn^{2+} adsorption) has been found using larger electrode samples. For both RuO_2 and IrO_2 coated electrodes, the voltammetric charge and the Zn^{2+} measured area were found to have a linear relationship with oxide loading. The correlation for RuO_2 was found to be 6.2 ± 0.6 Coul/m^2 and for IrO_2 it was 3.5 ± 0.5 Coul/m^2. The differences in the correlations for the two oxides has been attributed to differences in chlorine content of the two dioxides and consequential differences in grain boundaries and crystal defects.

Low overpotential exchange current densities of the ferric-ferrous couple were measured in concentrated solution (0.5 M Fe^{2+}, 0.5 M Fe^{3+}, 1 M HCl) at Pt, RuO_2 and IrO_2 RDE's. Significant corrections were necessary for ohmic effects, mass transfer effects, and nonuniform current distribution. The data show that the electrocatalytic activity of RuO_2 ($ks = 1.92 \times 10^{-3}$ cm/s) is comparable to that of Pt ($ks = 1.42 \times 10^{-3}$ cm/s) while the activity of IrO_2 ($ks = 1.21 \times 10^{-4}$ cm/s) is approximately an order of magnitude less than Pt. Since the measured free energy of activation was similar for all three substrates (5.4-5.8 Kcal/mole), a non-

binding interaction between the couple and the surfaces is suggested (i.e. outer-sphere transfer mechanism). The variation in exchange currents among the different substrates can be attributed to some extent on double layer effects but primarily to crystal structure differences.

The reaction orders of the ferric-ferrous couple in concentrated chloride solutions appear to be first order. However, measured cathodic and anodic transfer coefficients are 0.30 and 0.25 respectively for RuO_2 and 0.26 and 0.20 respectively for IrO_2. The low values of the transfer coefficients as compared to the theoretical predicted values could be a result of the following: (1) inapplicability of assumptions used in arriving at the theoretical value (e.g., metal electrodes, no specific adsorption or complexing of reactants); and (2) significant variation in overall free energy of activation, $\Delta G^{\ddagger}_{tot}$ due to its dependence on the overpotential because of the small values of $\Delta G^{\ddagger}_{c}$, the free energy of activation at zero overpotential.

Regarding the reproducibility of the metal oxide coatings, IrO_2 appears to be more stable than RuO_2. Also, the kinetic data at the IrO_2 surfaces was found to be more reproducible. In evaluating porous electrode theory by experiment, a very reproducible electrode surface is desirable so that kinetic rate expressions can be used with confidence. Consequently, it appears as though the IrO_2 coating is a more promising candidate for this application.

TABLE OF CONTENTS

1.0 INTRODUCTION

The consumption and production of energy are cyclic and often out of phase with each other. For example, the base load capacity of an electric utility is often only 50-65% of peak load. The current operating practice is to meet peak demands with low efficiency, costly auxiliary generators. Energy production can control the cycle as in the case of solar energy (direct, tidal, wind, etc.). During certain times there is an excess of energy available which is often dissipated while at other times the source is not present for energy production.

A recent study [1] specifies the leading contending batteries for bulk storage of energy as lead acid, zinc-halogen, metal-air, alkali metal sulfides and redox. Of these, the redox battery [2] shows significant merit because it is the only battery that has a potentially infinite life cycle and no depth of charge limitations. The redox battery employs two reacting couples (e.g. the iron couple and the chrome couple) whose products and reactants are separated by an anion permeable membrane and whose electrodes are inert and serve only as a catalytic site for electron transfer reaction. Although the redox battery is classified as low power density, it has the unique characteristic of separate sizing for power and capacity thus allowing unlimited capacity without adversely affecting power efficiency.

The basic developments necessary for the completion of the groundwork for redox batteries are: (1) the development of reproducible, long life electrodes (estimated at 10 to 20 years); (2) the development of long life, low resistivity ion exchange membranes; and (3) the development of advanced theoretical design equations.

Because of their high specific surface areas, porous electrodes will undoubtedly be used in any practical redox battery. Thus a more rigorous understanding of porous electrode theory will be invaluable in redox battery development. The majority of porous electrode studies have been conducted on some form of porous carbon or graphite. However, experimental verification of recent advances in porous electrode theory has been complicated by the instability and irreproducibility of carbon electrodes. Theoretical models for porous electrodes have been developed to the extent that these models can now be applied to the examination of battery systems [3]. Equations accounting for such specifics as double layer charging, adsorption of reactants, and mass transfer effects are available. However, experimental verification of theory has essentially been limited to confirmation of the existence of nonuniform reaction distributions. In addition, examinations of areas such as analysis of an entire electrochemical cell, prediction of the complete polarization curves of a battery, and optimization of a battery system have yet to be performed. Consequently, a need for the development of stable and reproducible porous electrodes exists. With the establishment of porous electrode theory, the development of more accurate design equations will be possible.

One of the goals of this research was to fabricate a stable and reproducible catalytic surface which can be placed on a well-defined porous matrix. Such a catalytic surface will then be available not only for the study of porous electrode theory, but also could become a candidate as a catalyst for redox battery electrodes. The catalysts chosen for evaluation were the dioxides of Ru, Ir, and Os. The choice of these transition metals was made because all form conductive metal oxides when present in the rutile crystal form. RuO_2 in solid solution with TiO_2 has already demonstrated its value as a dimensionally stable, long-life electrode in the chlor-alkali industry. Because of similar crystalline properties among the metal oxides, Os and Ir were expected to have comparable stability. However, the difference in the electronic factors of the metals suggests that the catalytic activity of each will vary. Therefore, the above catalysts were evaluated for activity and stability in concentrated solutions of the ferric-ferrous redox couple.

Because practical working solutions for redox batteries possess high reactant and supporting electrolyte concentrations (i.e., 1.0 to 4.0 M), some doubt exists as to the nature of the mechanism of charge transfer for the ferric-ferrous couple under these conditions. In dilute solutions, the outer-sphere electron transfer mechanism is applicable for the ferric-ferrous redox couple [4]. However, complexing of the above reactants with anions is known to occur in concentrated solutions [5]. Such complexing has been shown to catalyze both homogeneous and heterogeneous redox reactions for the ferric-ferrous couple [6,7]. Reported studies of the above redox couple in concentrated solutions are sparse, however, and limited investigations of the charge transfer mechanism have been performed. Thus, another aim of this research is to elucidate the mechanism of charge transfer for the ferric-ferrous redox couple in concentrated solutions.

In summary, redox batteries show promise as a means for future bulk energy storage. One step in the development of an economical redox battery will be the fabrication of long-life electrodes. This research focused on the development of a stable and reproducible catalytic surface suitable for porous electrode studies and also as a possible candidate as a catalyst for use in redox batteries. Because practical solutions for redox batteries are concentrated, the mechanism of charge transfer in these solutions also was examined.

2.0 LITERATURE REVIEW

To date, no studies dealing with the kinetics of the ferric-ferrous redox couple at RuO_2, IrO_2, or OsO_2 coated electrodes have been found. Almost all the past research has been conducted at electrodes of Pt, Au or some form of carbon and usually with a noncomplexing, nonadsorbing supporting electrolyte (e.g. $HClO_4$, H_2SO_4 or Na_2SO_4). The use of these electrolytes implies that the anions in solution do not form stable complexes with the reacting ions and that adsorption of these anions onto

the electrode surface is negligible. In addition, the reactant and supporting electrolyte concentrations were usually dilute (< 0.01 M) further reducing the importance of complexing and adsorption of the electrolyte.

A summary of the work performed by various researchers on the kinetics of the ferric-ferrous redox couple [8-12] is presented in Table 2-1. The standard rate constants were generally on the order of 10^{-3} to 10^{-4} cm/s with transfer coefficients closely approximating 0.5 for work performed in dilute reactant solutions with an indifferent supporting electrolyte. This work is not of primary interest and will not be discussed further. Instead the experiments performed by Miller [11] and Ateya and Austin [12] in concentrated solutions of HCl will be discussed.

Miller [11] examined the kinetics of the ferric-ferrous redox couple at edge-on-pyrolytic graphite (EOPG) rotating disk electrodes (RDE). Reactant concentrations ranged from 0.1 to 3 M for Fe^{+2} and from 0.1 to 2 M for Fe^{+3}; the ratio of Fe^{+2}:Fe^{+3} varied from 10:1 to 1:10. The HCl concentration was generally 1 M, 0.5 M being used in several experiments. The values of the rate constant in the above solutions ranged from $1x10^{-4}$ to $6x10^{-4}$ cm/s. From the values of the anodic and cathodic transfer coefficients, Miller postulated that the charge transfer mechanism was a simple one-step electron exchange reaction. However, the values for the anodic transfer coefficient varied from 0.21 to 0.66 while those for the cathodic transfer coefficient varied from 0.30 to 1.07. This variation places some doubt on the conclusion that the actual transfer coefficients are equal to 0.5 and thus that a simple electron transfer mechansim is applicable. Although complexing of the reactants with chloride ion was mentioned, its effect on the charge transfer mechanism was not considered.

Ateya and Austin [12] studied the ferric-ferrous system at reactant concentrations of ~ 0.01 N in 4 N HCl solutions. The measured rate constants at EOPG and basal plane pyrolytic graphite (BPPG) were $5.2x10^{-4}$ cm/s and $1.5x10^{-4}$ cm/s, respectively. The anodic and cathodic transfer coefficients were calculated to be 0.4 ± 0.04 and 0.6 ± 0.04 respectively. Based on their data, Ateya and Austin concluded the reaction to be a first order, simple one-step electron exchange reaction for currents less than 70% of the limiting current values. The apparent activation energy was calculated to be 11.5 kcal/gmole and 9.5 kcal/gmole at EOPG and BPPG, respectively. The differences in the activation energies were not discussed.

TABLE 2-1

Summary of Literature Kinetic Data for Fe^{2+}/Fe^{3+} Redox Couple

Medium	Reactant conc.	Electrode Material	Standard Rate Constant	Cathodic Transfer Coefficient	Reference
0.5M H_2SO_4	0.002-0.01M	Pt	7×10^{-3}	0.5	8
		Au	10×10^{-3}	0.5	
0.1M H_2SO_4	0.001M	Pt	4.3×10^{-3}	0.6	9
1.0M H_2SO_4	0.001M	Carbon Paste	5.4×10^{-5}		
0.1M HCl	0.001M	Carbon Paste	7.4×10^{-5}		
0.45M H_2SO_4		Pt	4.3×10^{-3}	0.5	10
0.45M H_2SO_4		Glassy Carbon	8.6×10^{-4}	0.5	
4.0N HCl	0.093M Fe^{2+} 0.096M Fe^{3+}	EOPG* BPPG**	5.2×10^{-4} 1.5×10^{-4}	0.6	12
1.0M HCl	0.2-3M	EOPG	1×10^{-4} to 6×10^{-4}	0.3 to 1.07	11

*Edge-on-pyrolytic graphite

**Basal plane pyrolytic graphite

3.0 THEORY

The principal emphasis in electrochemical studies is usually placed on the mechanism and rate of charge transfer between the reactants in the electrolyte and the electrode surface. Several reaction mechanisms can usually be postulated for a given reaction. The choice of the most probable reaction scheme can usually be made, however, by measurement of kinetic parameters such as reaction orders, free energy of activation, and transfer coefficients. These parameters are determined by measuring the reaction rate as a function of the driving force.

The theory of charge transfer mechanisms, the effect of reactant complexes and the basis of kinetic rate expressions are presented in Appendix A. Also in Appendix A is the theoretical basis for the corrections made to experimental data to account for concentration effects, non-uniform reaction distributions and solution ohmic drop. Finally, the theory employed in estimating the kinetic parameters is given in Appendix A.

4.0 EXPERIMENTAL

4.1 Electrode Preparation

Transition metal dioxide coatings were prepared on titanium substrates by thermal decomposition of the hydrated metal chlorides. For adsorption surface area measurements, the coatings were deposited on 1/32" thick sheets of commercial grade titanium (United Titanium Corp., Wooster, Ohio).

In the case of ruthenized electrodes, the coating method was similar to that used by O'Grady, et al. [23]. After degreasing, polishing to a mirror finish, and etching in concentrated HCl (at 80°C for ~ 1.5 minutes), the titanium was washed thoroughly in deionized water. This was followed by repeated application of a solution of $RuCl_3$ dissolved in butyl alcohol and HCl (0.6 M $RuCl_3$, 9.4 ml butanol, 0.06 ml conc. HCl; diluted with same solvent for lighter loadings). After each application, the coating was air dried for 5 minutes, followed by further drying at 110°C for 5 minutes, then baked at 350°C for 10 minutes. Initial air drying improved the uniformity of the coatings. The first two steps evaporated the solvent while the third effected the decomposition of $RuCl_3$ to RuO_2. When the desired loading of ruthenium had been achieved, the furnace temperature was raised to 450°C for 1 hour for the final heat treatment. This procedure resulted in the formation of the rutile crystal structure from amorphous RuO_2. Loadings on the order of 10^{-5} moles Ru/cm^2 of geometric area have been achieved after 6 coating applications using a 0.6 M Ru solution.

The RuO_2 coatings prepared in the above manner have been examined by powder x-ray diffraction and by SEM. X-ray diffraction patterns were obtained using copper radiation of wavelength 1.54050 A. The characteristic peaks for both Ti and RuO_2 were observed. The interplanar spacings observed for Ti were 2.24, 2.55 and 2.34 angstroms while those for RuO_2 were 1.69 and 3.19 angstroms. The peak expected at 2.52 angstroms for RuO_2 was sometimes masked by those of titanium depending on the loading of the dioxide coating. No evidence of the presence of TiO_2 was observed. SEM photomicrographs shown in Figure 4-1 are of ruthenium dioxide coatings applied to polished titanium substrates which have been etched for 2 and 5 minutes. The mud cracked surface is most likely caused by volume contraction during evaporation of the solvent. A similar surface structure was observed on commercial ruthenized titanium electrodes [35].

Preparation of IrO_2 films were successfully accomplished by following the procedure used for preparing ruthenized electrodes. The rutile crystal structure of IrO_2 was confirmed by x-ray diffraction; characteristic peaks appeared at interplanar d-spacings of 3.17, 2.58, and 1.70 A. SEM examination of the IrO_2 films revealed the same mud-cracked surface as observed on RuO_2 films.

Having established a procedure for preparing RuO_2 and IrO_2 films on a titanium substrate by the decomposition of hydrated metal chlorides, the preparation of OsO_2 electrodes was attempted. Preparation of OsO_2 was first attempted by following the procedure used for ruthenized electrodes. However, during the 350°C baking step, it appeared as though the product was the highly volatile OsO_4 which is known to be formed from oxidation of finely divided OsO_2 in air [24]. The oxidation temperature was lowered in 20°C increments until 230°C, when it was established by visual inspection and weight change measurements that indeed an oxide coating existed on the substrate. Although EDAX scans did confirm that osmium was present (characteristic peaks at 1.90, 8.9, 10.3 and 10.5keV), x-ray diffraction did not find the rutile structure present. In an attempt to convert to the rutile structure at 350°C (the temperature reportedly where HCl soluble OsO_2 transforms to insoluble OsO_2 [25]), the coating again volatilized. Further attempts to convert the osmium oxide to the rutile structure, such as by annealing in an inert atmosphere, were not attempted.

As a sidelight, attempts to apply ReO_2 films to a titanium substrate met with results similar to those of osmium.

4.2 Determination of Electrode Surface Area

The determination of the electrochemically active surface area is important in evaluating the intrinsic activity of electrode materials. Several techniques are available for estimating the active or true surface area: (1) Zn^{2+} ion adsorption; (2) B.E.T. measurement with krypton; (3) measurement of double layer capacitance; and (4) cyclic voltametry. The Zn^{2+} ion adsorption

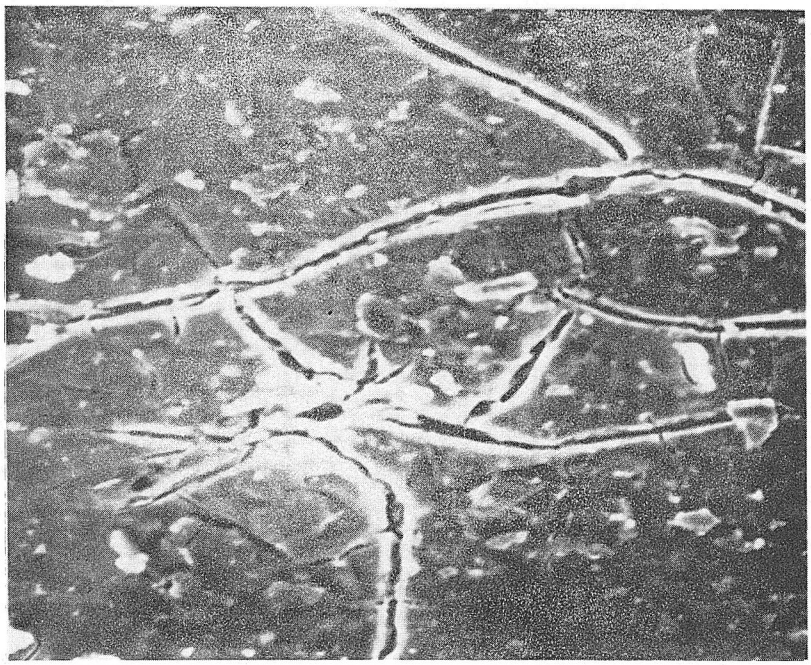

(a)

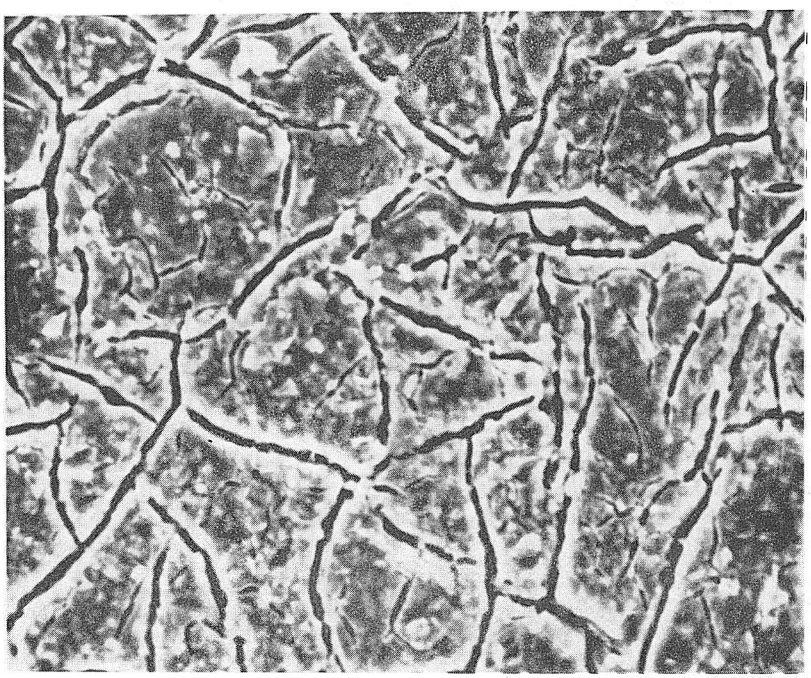

XBB 833-1847

(b)

Figure 4-1. SEM Photomicrographs (x500) of ruthenium dioxide coatings applied to polished titanium substrate etched in HCl at 80°C:
(a) etched 2 minutes with loading of 17.3 g Ru/m^2;
(b) etched 5 minutes with loading of 16.7 g Ru/m^2.

technique developed by Kozawa [26] has previously been used by O'Grady, et al. [23], to obtain an estimate of the true to apparent surface area ratio of RuO_2 coatings on a titanium substrate. This method is preferred over the more established B.E.T. measurement since the latter may include pores that are not electrochemically active.

The measurement of the double layer capacitance as a means of determining the active surface area was suggested by Salkind [27] and a review of this technique as applied to porous electrodes has been provided by Newman and Tiedemann [3]. This technique works best when Faradaic reactions do not occur. However, at the transition metal oxide electrodes of this study, the cyclic voltamograms are characterized by a very broad cathodic and anodic region, the cause of which is attributed to surface redox reactions. These Faradaic reactions are significant as compared to double layer charging currents. Therefore we did not use this method for measuring our electrode areas.

Burke [28] utilized the voltammetric charge obtained by cyclic voltammetry (due to surface redox reactions) to obtain a value for the true surface area. This technique is ideal for estimating the true surface area of an RDE since the geometrical area is small. In our work a steady state cyclic voltammogram of the test piece was obtained in 1 M H_2SO_4. The potential was cycled at 20 mV/s within the range of 0.05 and 1.0 V vs SCE at 25°C. The cathodic and anodic charge was usually within several percent of the average. In this technique, the specific charge per unit true surface must be known. Burke found this value for ruthenized titanium electrodes by correlating his measured charge data with B.E.T. surface area data. For this work we used the Zn^{2+} adsorption technique as the primary standard. The details of this technique are given below.

The Zn^{2+} adsorption method is based on the ability of Zn^{2+} to exchange with H^+ which is bound to O^{2-} of the surface coating [23]. The technique involves immersing an electrode in a known volume of 0.5 M NH_4Cl, 0.001 M ZnO solution at a pH of approximately 7. The electrode remains in the solution until equilibrium is obtained. It was found that although equilibrium adsorption was rapidly approached after several hours of immersion, it took overnight immersion before equilibrium was reached. Consequently, most measurements were taken after the electrodes were immersed in solution overnight. The concentration of Zn^{2+} ions in solution was determined before and after by titrating with an EDTA solution using Erichrome Black T as the indicator. The suggested pH for this titration ranges from 6.8-10 [29]. The most consistent results were obtained at a pH of 10. A blank run was performed to determine whether Zn^{2+} ions were being absorbed into the Plexiglass container; no adsorption of Zn^{2+} ions was measured. Our experimental error with this technique was estimated to be ~ $\pm$ 15%. The calculation of surface area was based on assuming a zinc ion surface area of 17$(A)^2$/ion [23].

4.3 Electrokinetic Measurements

The electrochemical cell used for obtaining kinetic data was designed based on the work of Prater and Adams [30], Opekar and Beran [18], and Riddiford [17]. Although the cell was equipped with capability for in-situ preelectrolysis of solutions [31], this was not used in our studies. The reference capillary tip was placed at the outer edge of the disk electrode.

The platinum electrode used in this study was a commercial rotating disk electrode (RDE) supplied by Pine Instruments (Grove City, PA, Dia = 0.764 cm). Another RDE was designed and constructed and has removable titanium electrodes (Dia = 0.6 cm). The oxide coatings were applied to the titanium substrate, then the electrode was mounted in the teflon insulating cylinder. Details of the cell and electrode design are reported in the thesis of J. A. Adams [32].

Electrochemical measurements were carried out in solutions of ferric and ferrous ions in 1 N HCl. Ferric and ferrous chlorides supplied as reagent grade salts (Fisher Scientific, Pittsburgh, PA) were used as-received. Solution concentrations were determined by titrating with prenormalized titanous chloride solution. Reagent grade hydrochloric acid was used as-received. The water used in these experiments was deionized, then distilled, then double oxidative distilled as recommended by Powers [33].

Electrokinetic measurements were made following an established protocol. In the case of the Pt electrode, the protocol was:

(i) Mechanically pretreat the surface by polishing with 0.05 μ alumina for one minute. In one molar sulfuric acid the following electrochemical pretreatment was applied: 10 seconds at 1.56 V vs SCE, 30 seconds at 0.96 V, 30 seconds at -0.19 V; repeated 5 times.

(ii) Obtain a steady state voltammogram to be used for estimating surface roughness from H-adsorption charge [34] (still in 1 M H_2SO_4).

(iii) Transfer electrode to cell with working solution.

(iv) Make current interrupt measurements to estimate IR drop between electrode and capillary tip.

(v) Obtain steady state overpotential current data. The following sequence was used; open circuit, anodic overpotential and measurement, open circuit, cathodic overpotential and measurement etc.; repeat at numerous overpotentials and for several rpm's.

(vi) Obtain anodic and cathodic limiting current data at the same rpm's that kinetic data were taken.

(vii) Make current interrupt measurements again.

(viii) Obtain steady state voltammogram in 1 M H_2SO_4 to check for surface instability after kinetic measurements.

In the case of the ruthenized and irididized titanium electrodes, steps (i), (ii) and (viii) were:

(i) & (viii) In 1 M H_2SO_4, obtain a steady state voltammogram for estimating surface area -see section 4.2.

(ii) Hold electrode at 0.865 V vs. SCE for ~ 5 minutes.

The other steps were the same as for the Pt electrode.

The electrokinetic overpotential data was corrected for IR by using the current interrupt data. The surface concentrations were corrected by using the measured limiting current data (see Appendix A). For obtaining free energy of activation and reaction order data, the overpotential had to be maintained constant. This required the establishment of the controlled overpotential by trial and error with IR correction.

5.0 RESULTS AND DISCUSSION

In this chapter the experimental results are presented and the interpretation of the data is discussed. Only a summary of the calculated values is presented. The raw data and calculation details are presented elsewhere [32].

5.1 Surface Area Correlations

Initially, experience measuring electrode surface areas has been acquired using commercial ruthenized titanium electrodes ($Ru_xTi_{1-x}O_2$ where x is believed to be 0.3). Figure 5-1 presents two voltammograms of a ruthenized titanium electrode and Table 5-1 summarizes some results of surface area measurements. The surface area of a ruthenized electrode as measured by the voltammetric charge correlation of Burke [28,43] gives a roughness factor (i.e. real area: apparent area) of 247 which is reasonable for these electrodes [35]. Area measurement by Zn^{2+} adsorption (although not of the same samples) gave a roughness factor of 162-169. Since Burke's voltammetric charge correlation is based on B.E.T. data (which includes contributions to the area from micropores which are not necessarily electrochemically accessible) these results appear to be consistent. The cathodic and anodic charge under the voltammogram agree quite well with each other (see Table 5-1) and they remain essentially constant after repeated cycling. However, after extended exposure to sulfuric acid solution, there is an increase in voltammetric charge as shown in Figure 5-1. The increase in charge is a direct result of greater true surface and this was verfied optically by SEM examination.

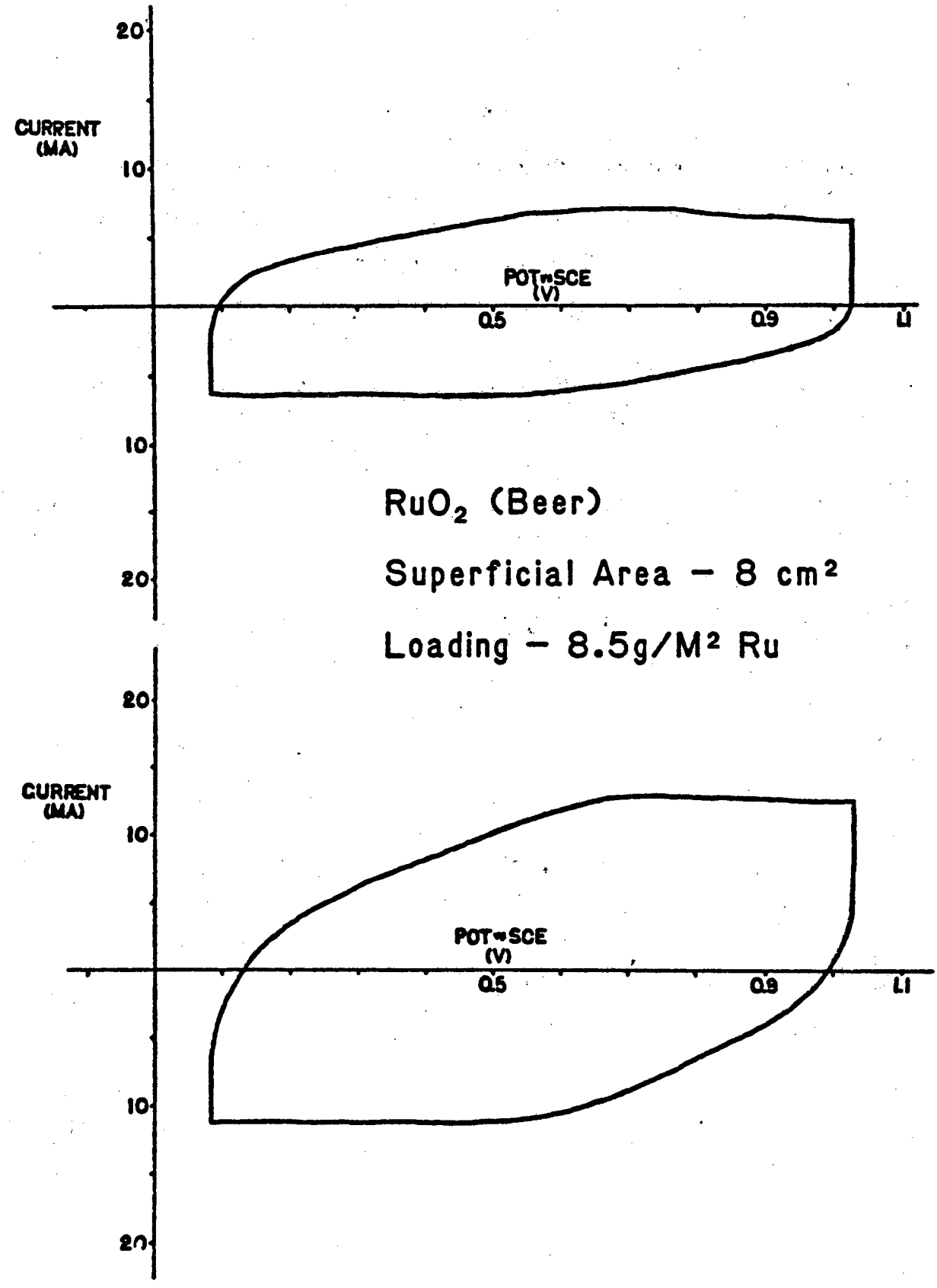

Figure 5-1: Surface area traces of beer electrode before (upper) and after 6 days in 1 M H_2SO_4 (20 mV/s).

TABLE 5-1

Summary of Results of Measuring Electrode Surface Area of Commercially Supplied Electrodes* by Voltammetric Charge Area Technqiue

(based on 1.35 Coul/m)

Metal Oxide coating	Loading moles M/cm of $M_x Ti_{1-x} O_2$	True Area / apparent area	% Diff Cath-Anod Areas
RuO_2 initial	$.85 \times 10^{-5}$	247	1.4
RuO_2 aged	$.85 \times 10^{-5}$	401	7
IrO_2 initial	$.44 \times 10^{-5}$	240	4
RhO_2 initial	$.36 \times 10^{-5}$	75	3.4
RhO_2 aged	$.36 \times 10^{-5}$	65	5

*Supplied by Diamond Shamrock Corporation, Painesville, Ohio.

Therefore, it was concluded that surface area measurements prior to and following the taking of kinetic data was necessary [44].

Table 5-1 also shows the results of some surface area measurements made on other commercial electrodes that were available in our lab. It was encouraging to note that the iridized electrode behaved similar to the ruthenized electrode, therefore the voltammetric charge technique was thought to be applicable to that oxide as well.

An interesting comparison of a mixed oxide electrode ($Ru_{0.3}Ti_{0.7}O_2$ with 8.24g Ru/m^2) and a ruthenized titanium electrode (17.3g Ru/m^2), both prepared in our lab, revealed an identical roughness factor of 150 based on the voltammetric charge technique [45]. Furthermore, the charge-sweep rate response for both electrodes are the same (see Figures 5-2) and are similar to that reported by Burke [28]. This result appears to support the view that less precious metal may be employed in the mixed oxide form with no decrease in true surface area.

Correlations between surface area determined by Zn^{2+} adsorption and voltammetric charge measured in 1 M H_2SO_4 were developed for both RuO_2 and IrO_2 electrodes. As shown in Figure 5-3 and 5-4, both the surface area and the charge appear to have a linear relationship with the oxide loading. The surface area-charge correlations are shown in Figure 5-5 and 5-6 and the data are summarized in Table 5-2. The correlation for RuO_2 and IrO_2 electrodes are 6.2 ± 0.6 and 3.5 ± 0.5 $Coul/m^2$, respectively. The value for RuO_2 compares to 1.35 $Coul/m^2$ from Burke et al. [28] which is based on B.E.T. data and the same voltammetry conditions. These results indicate that the B.E.T. surface of RuO_2 is approximately 4.6 times the Zn^{2+} area. (Recall that Zn^{2+} measurements estimate electrochemically active area while B.E.T. measurements also include inaccessible micropores). This ratio is in reasonable agreement with the ratio of 3.4 (B.E.T. area: Zn^{+} area reported by O'Grady et al. [23]) for a ruthenium loading of 10^{-5} moles/cm^2 of geometric area.

The charge correlation for the RuO_2 electrode is about twice the charge correlation of the IrO_2 electrode. A possible explanation for the difference in the above values for IrO_2 and RuO_2 may be found by examining the crystalline structures of the dioxide films. Pizzini, et al. [36] determined that for RuO_2 films prepared by

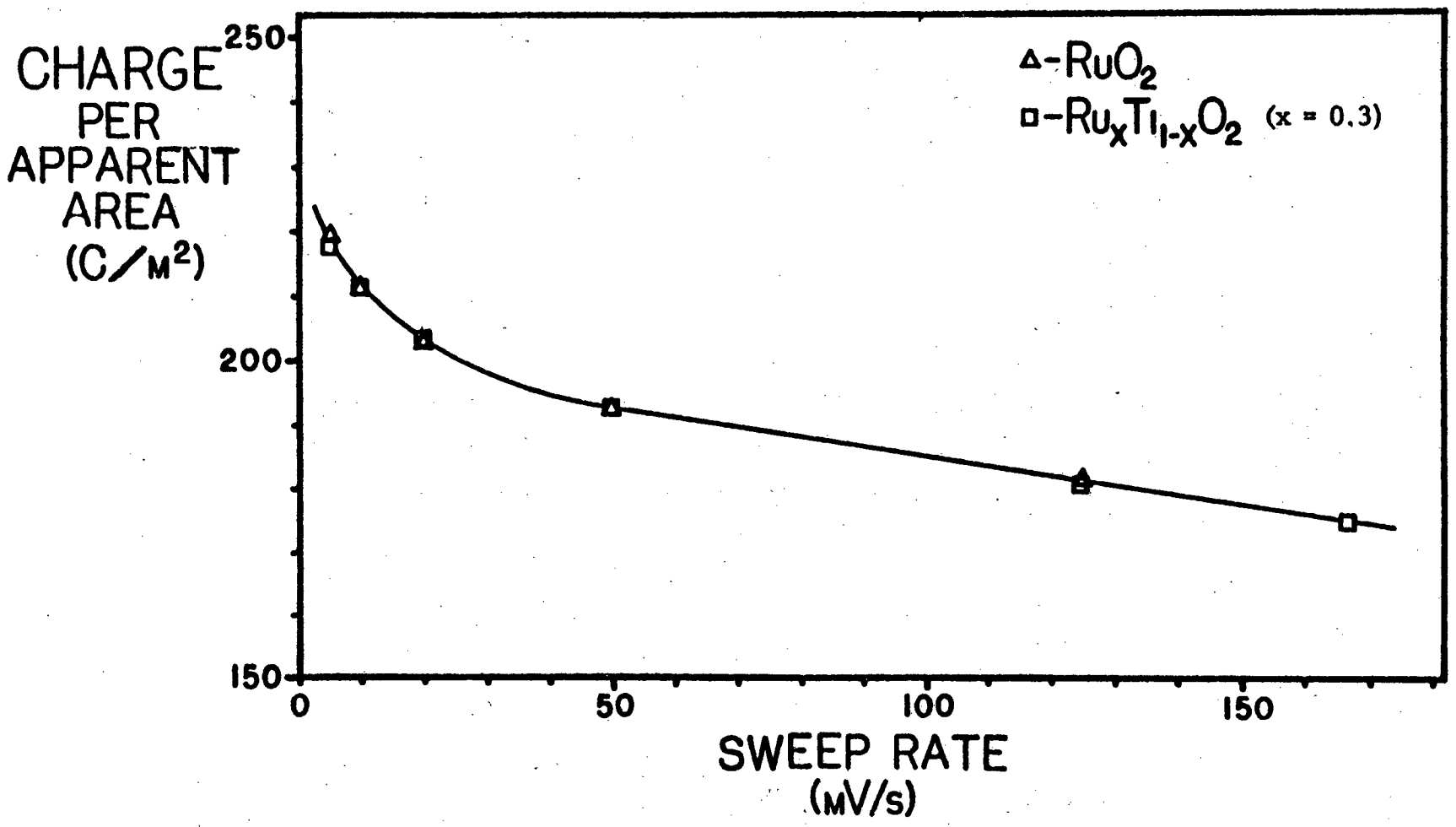

Figure 5-2: Comparison of voltammetric charge data for mixed oxide and ruthenized titanium electrodes.

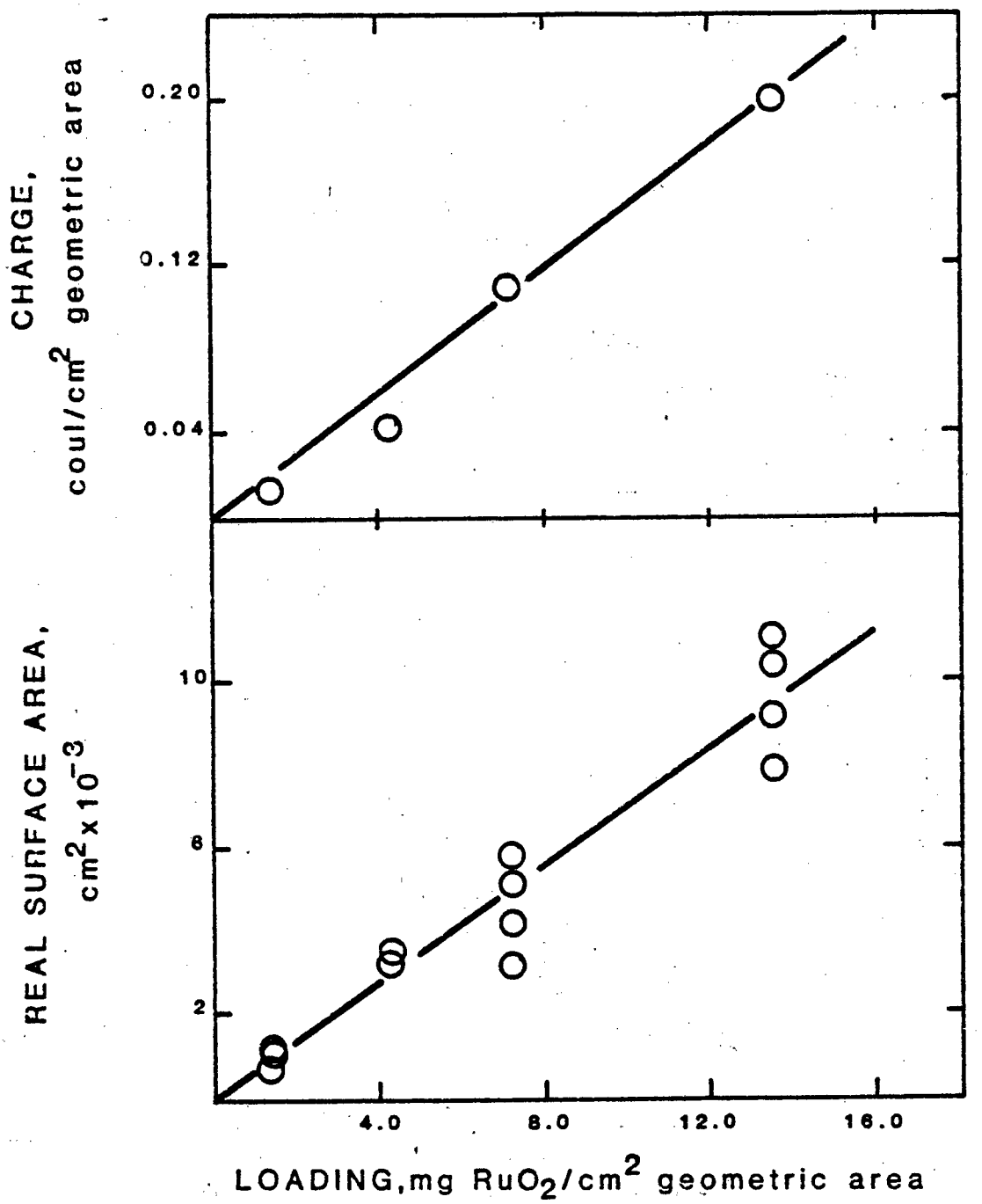

Figure 5-3: Voltammetric charge and real surface area correlated with RuO_2 loading on a titanium substrate.

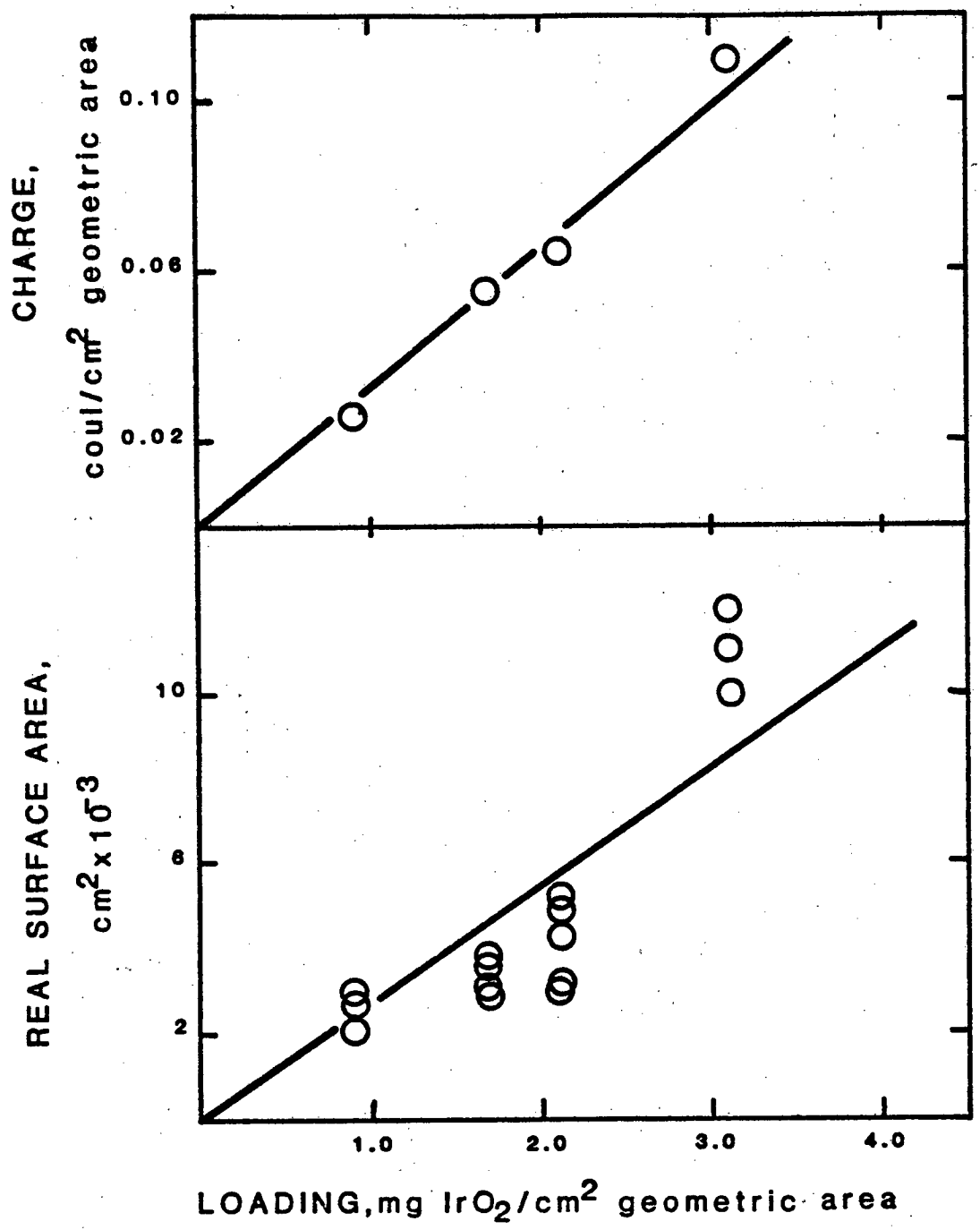

Figure 5-4: Voltammetric charge and real surface area correlated with IrO_2 loading on a titanium substrate.

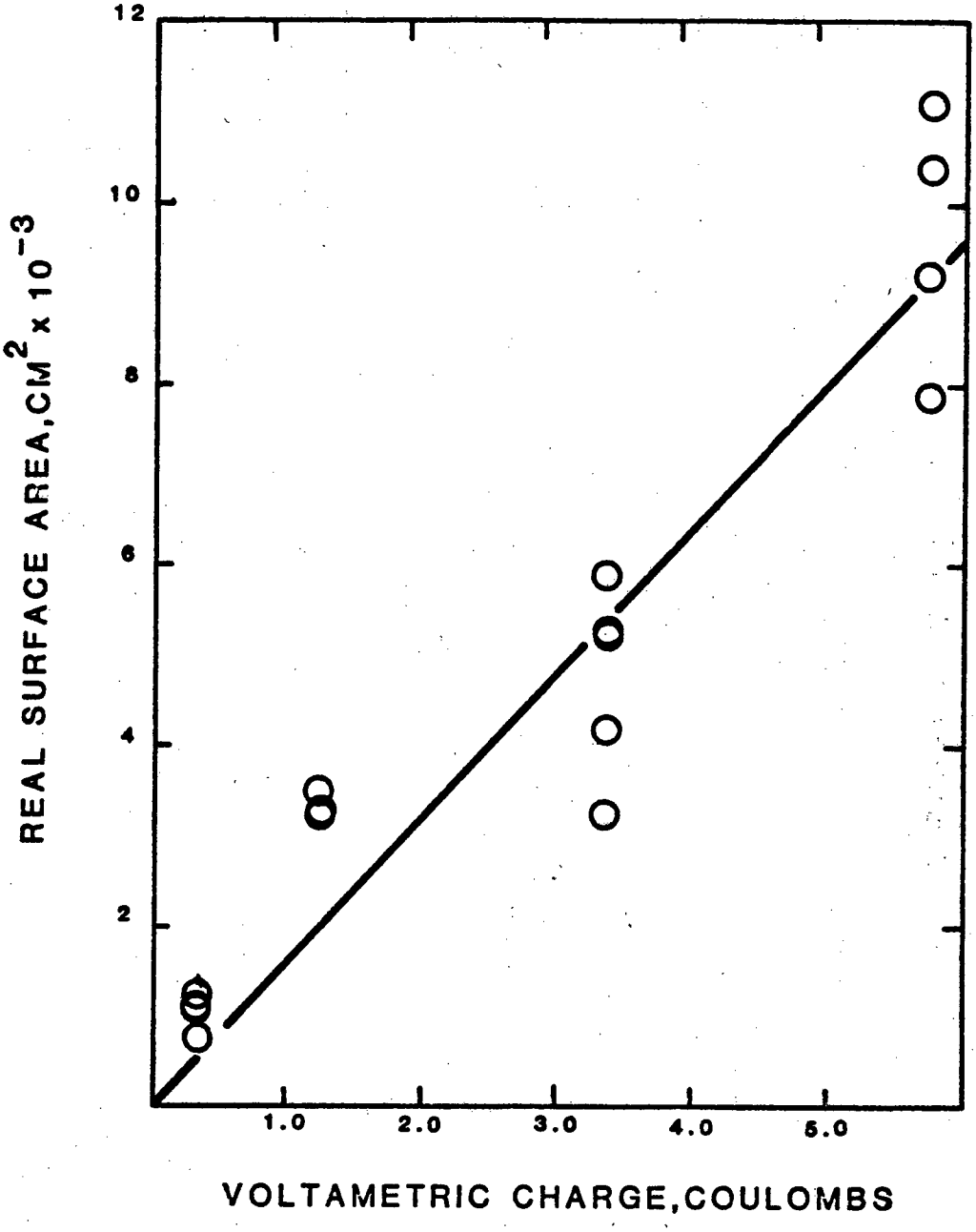

Figure 5-5: True area correlated with voltammetric charge for ruthenized titanium electrodes.

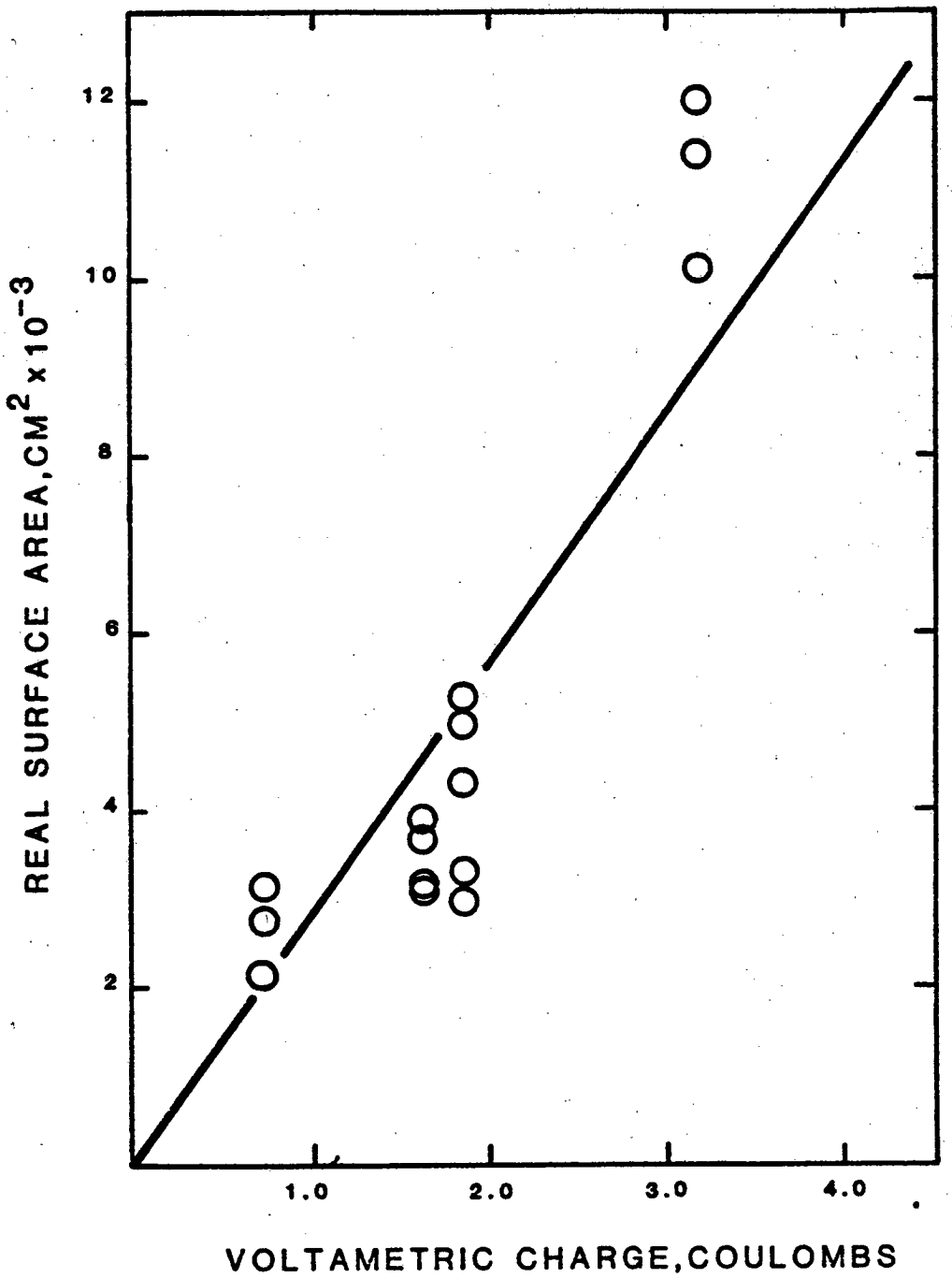

Figure 5-6: True area correlated with voltammetric charge for iridized titanium electrodes.

TABLE 5-2

Surface Area Correlations

MO_2	Charge/Loading Coul/mg	Surface Area/Loading cm^4/mg	Surface Area/Charge $cm^2/Coul$	# Data Pts.
RuO_2	0.015 ± .001	710 ± 60	1640 ± 170	16
IrO_2	0.033 ± .001	2760 ± 490	2890 ± 430	15

NOTE: plus and minus are for 95% confidence interval.

thermal decomposition of $RuCl_3 \cdot xH_2O$ and annealed at 450°C, the chlorine content was approximately 3 to 4% by weight. Thus the crystal structure is nonstoichiometric. Newkirk and McKee [37], in their investigation of the thermal decomposition of Rh, Ir, and Ru chlorides to form the pure metals, found that the dechlorination of Ir and Ru was complete at 680°C and approximately 440°C, respectively. Based on these dechlorination temperatures, it seems reasonable to assume that IrO_2 films prepared by thermal decomposition of $IrCl_3 \cdot xH_2O$ and annealed at 450°C will contain chlorine and will be nonstoichiometric. Furthermore, because the dechlorination of Ir occurs at a higher temperature than Ru, the chlorine content of IrO_2 could be even higher than that of RuO_2. The postulated increase in chlorine content would increase the number of grain boundaries and defects in the IrO_2 film over that present in a RuO_2 film. The increased number of defects would result in an increased number of Ir atoms being exposed. During Zn^{2+} adsorption to measure the surface area, a greater number of Zn^{2+} ions could adsorb and thus the surface area of IrO_2 should be larger than that of RuO_2. Thus the value of the surface area/mg of dioxide loading should be greater for IrO_2 than for RuO_2. This is shown to be true in Table 5-2. Although the charge/mg dioxide loading correlation for IrO_2 is approximately 2 times that for RuO_2, the surface area/mg dioxide loading correlation for IrO_2 is approximately 4 times that of RuO_2. Thus it appears that the majority of the difference in the surface area-charge correlations for the two dioxides lies in the increased surface area of IrO_2 films. The increased surface area could be a result of a larger chlorine content in the IrO_2 crystal structure.

5.2 Stability of Oxide Coatings

It was found that the shape of the voltammogram of the RuO_2 electrode became distorted after immersing in chloride working solutions. The shape distortion increased after taking kinetic data. For an example, see Figure 5-7. This change did not occur with the IrO_2 electrodes thus indicating that the IrO_2 coating is more stable and perhaps more reproducible which is important for porous electrode studies.

The instability of the RuO_2 films as compared to the IrO_2 films can be explained by examination of the crystal structure of the dioxides. During the decomposition of the metal chlorides to form the metal dioxides, the water of hydration is partially retained in RuO_2 coatings but is not is IrO_2 coatings [37]. Okamoto and Shibata [38], studying passive films on stainless steel, noted that anion adsorption onto the surface resulted in the loss of water of hydration from the passive film. In the case of RuO_2, exposure to the working solution may have resulted in the loss of trapped water molecules from the dioxide crystal structure due to chloride ion adsorption. With the loss of the water molecules from the RuO_2 films, the possibility of a structural rearrangement to form single crystals of RuO_2 exists. Trasatti and Buzzanca [39] studied RuO_2 films prepared by thermal decomposition of the metal halides and

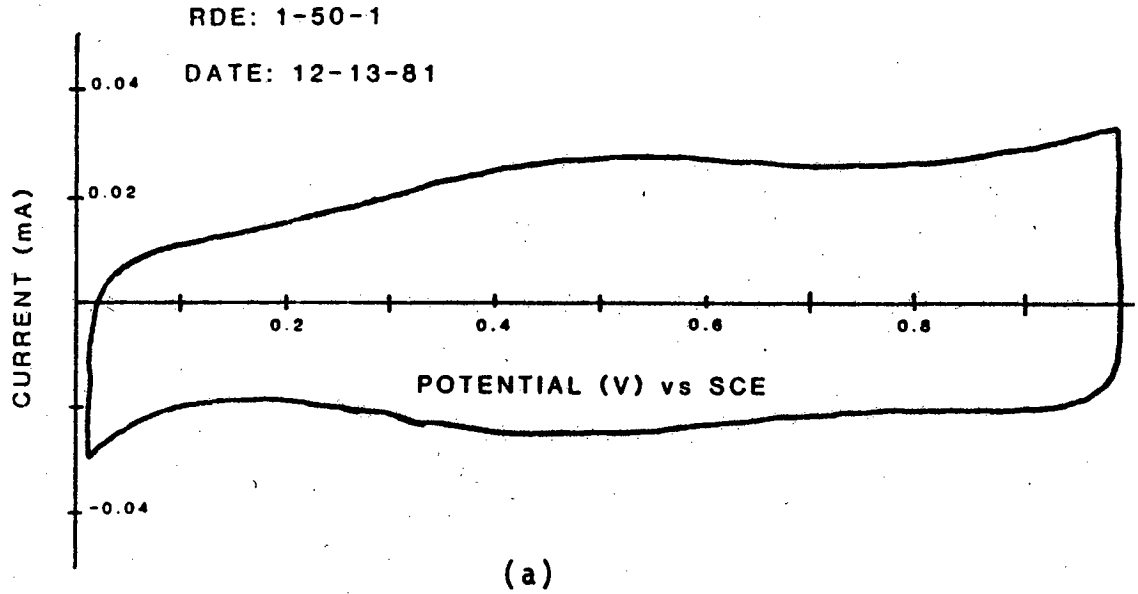

(a)

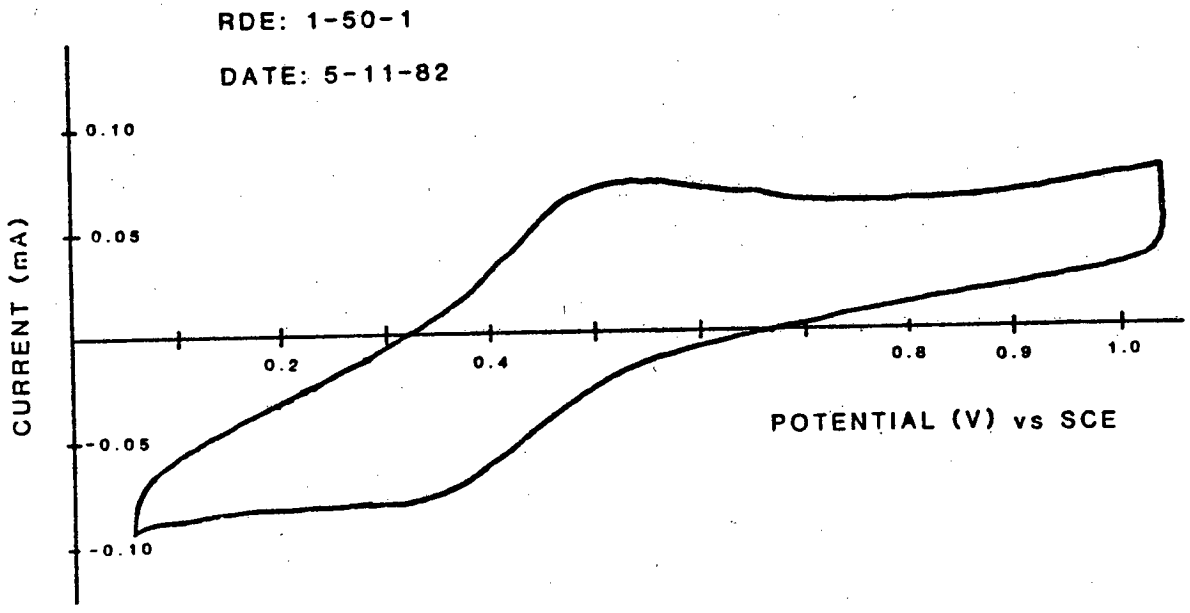

(b)

Figure 5-7: i/E curve for RuO_2 film on titanium (a) before and (b) after exposure to chloride medium; voltammogram taken in 1 M H_2SO_4 at 20 mV/s.

RuO_2 single crystals prepared by vapor transport of Ru and O_2. They performed voltammetric sweeps in 1 M $HClO_4$ for both RuO_2 films and single crystals, these sweeps are reproduced in Figure 5-8. In Figure 5-7, voltammetric sweeps in 1M H_2SO_4 of RuO_2 films produced in this lab before and after exposure to chloride medium are shown. Comparison of Figure 5-8a with Figure 5-7a shows the similarity between RuO_2 films prepared by Trasatti and Buzzanca and those prepared in this research. Comparison of Figure 5-8b with Figure 5-7b shows that there is a definite similarity in the voltammetric sweeps between single crystals of RuO_2 and the RuO_2 films of this research after exposure to chloride medium. It should be noted that this change in the voltammetric sweeps was not observed on RuO_2 electrodes used in the development of the surface area-charge correlation which were exposed only to 1 M H_2SO_4. Also the change appears to be irreversible. Thus the adsorption of chloride ions onto the RuO_2 film may result in the loss of trapped water molecules which in turn may result in the structural rearrangement of the RuO_2 film to single crystals of RuO_2. Also, the stability or IrO_2 films in chloride medium could be explained by the lack of water of hydration in the dioxide film and therefore its indifference to chloride ion adsorption.

5.3 Electrocatlytic Activity

Low overpotential measurements of exchange current densities were made in concentrated solutions (0.5 M Fe^{+}, 0.5 M Fe^{3+}, 1 M HCl) at Pt, RuO_2 and IrO_2 RDE's. Data corrected for IR and nonuniform current distribution are reported in Table 5-3. There was considerable scatter in the data for the RuO_2 electrodes as compared to the data for the IrO_2 electrode. However, an examination of Table 5-3 reveals that the activity of RuO_2 is consistently over one order of magnitude greater than that of IrO_2 and on the same order as Pt. One possible explanation for these results can be presented and relies on arguments based on the crystalline structure of the dioxide films.

IrO_2 and RuO_2 are metallic conductors. The electrons in the d bands are responsible for this conductivity. The radius of the metallic cations and the distance between them are such that the inner d-orbitals overlap [39]. In addition, these dioxides have incompletely filled d-orbitals [40]. The combination of orbital overlapping and unfilled orbitals gives rise to the metallic conductivity.

As shown earlier, trapped water and chlorine molecules in the crystalline structure of RuO_2 resulted in the formation of nonstoichiometric dioxide films. The effect of the nonstoichiometry is to reduce the amount of overlapping of d-orbitals and increase the distance between metal atoms by development of numerous grain boundaries; the effect on physical properties is quite apparent. For example, the conductivity of RuO_2 films prepared by thermal decomposition of $RuCl_3 \cdot xH_2O$ is approximately 3 orders of magnitude less than

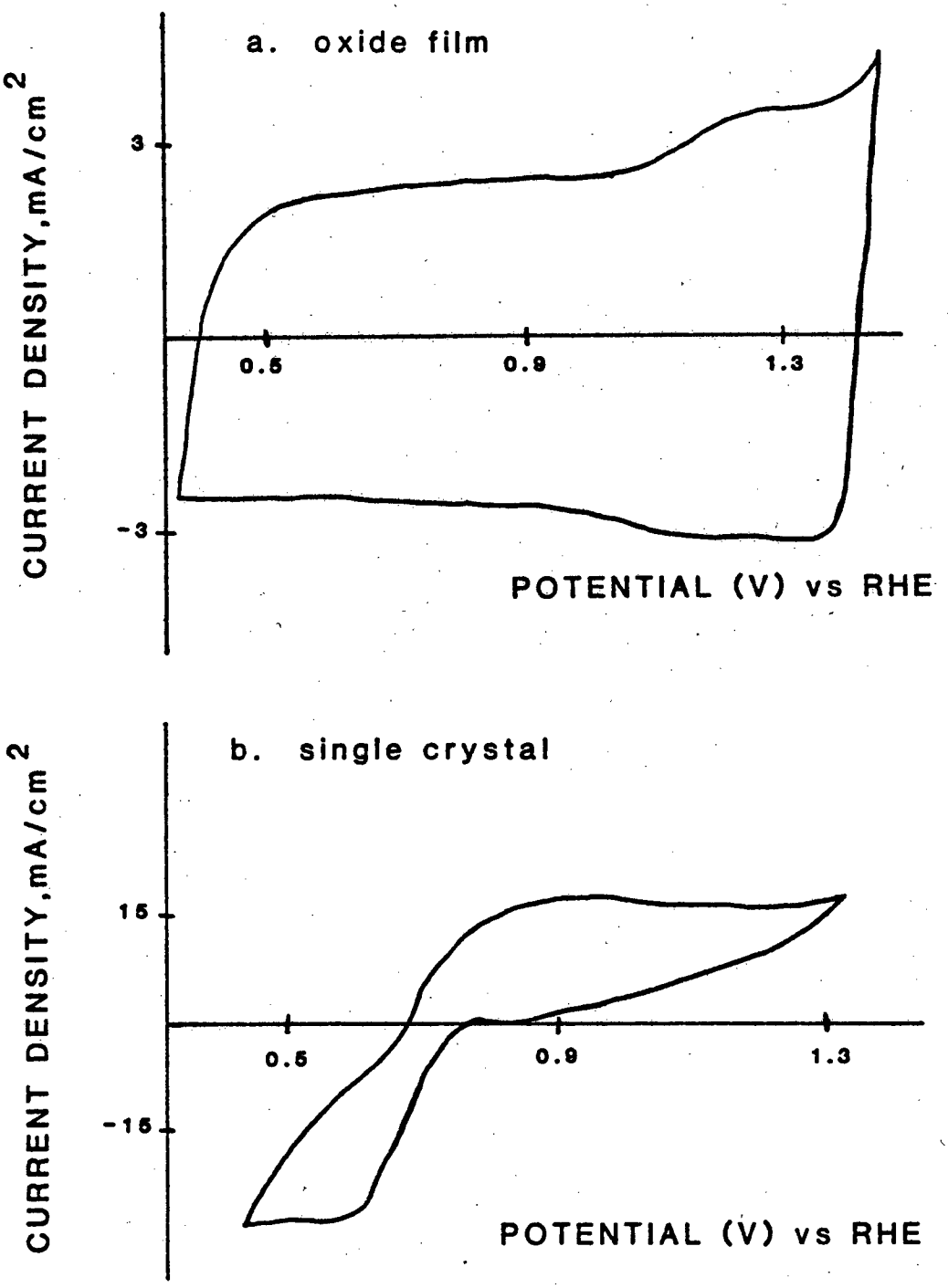

Figure 5-8: i/E curves for films and single crystals of RuO_2 in 1 M $HClO_4$ at 40 mV/s. Redrawn from Reference [39].

TABLE 5-3

Electrokinetic Data of Pt, RuO_2, and IrO_2*

Electrode	Roughness Factor	Newman** Correction $i_{o,true}/i_{o,app}$	i_o‡ (A/cm² real area)x10²	k_s+‡ (cm/s)x10³	Transfer Coefficients‡ Anodic	Cathodic
Pt	1.6	1.9	6.87	1.42		
RuO_2(1-50-1)	7.8	3.4	15.3	3.17	0.248±0.005	0.297±.004
RuO_2(2-28-1)	16	3.7	8.99	1.86		
RuO_2(2-28-1)	17	3.0	3.57	0.74		
			9.29 ± 5.87	1.92 ± 1.22		
IrO_2(2-10-1)	49	2.3	0.612	0.127	0.203±.009	0.261±.018
IrO_2(2-10-1)	52	2.2	0.499	0.103		
IrO_2(2-29-1)	120	3.0	0.639	0.132		
			0.583 ± 0.074	0.121 ± 0.016		

*RPM was 3500 and working solution was 0.5 M Fe^{2+}, 0.5 M Fe^{3+}, 1 M HCl in all cases.

**$(\alpha^{+} + \alpha^{+})$ taken as unity

+Simple one-step electron transfer assumed

‡± values represent one standard deviation.

that of single crystals prepared by vapor phase transport of Ru and O_2 [36,40]. Consequently, the variation of the non-stoichiometry of the crystals caused by loss of trapped water could be the cause of the apparent variation of the catalytic activity of RuO_2 films.

As discussed earlier, the chlorine content of IrO_2 films was postulated to be higher than that of RuO_2 films. The increased chlorine content would result in a greater number of grain boundaries and defects. Therefore, the interaction of d-orbitals in IrO_2 coatings would be lower than that of RuO_2 films. Pizzini, et al. [36] demonstrated that the decrease in d-orbital interaction due to increased chlorine content in RuO_2 films results in a decrease in the electrical conductivity. Thus the higher chlorine content postulated for IrO_2 films could result in a larger decrease in the electrical conductivity than that experienced by RuO_2 films. The lower electrical conductivity would thus result in lower apparent electrocatalytic activity. The lower catalytic activity and higher surface area of IrO_2 films as compared to RuO_2 are both consistent with the concept of a higher chlorine content of IrO_2 films.

5.4 Free Energy of Activation

In order to elucidate the role of electrode substrate and to determine whether charge transfer mechanisms in these concentrated solutions are via outer-sphere electron transfer, the free energies of activation were measured in solutions of 0.5 M Fe^{2+}, 0.5 M Fe^{3+}, 1 M HCl at Pt, RuO_2 and IrO_2 RDE's. Data for these electrode surfaces are presented in Figure 5-9 and the results are tabulated in Table 5-4. The free energies of activation at zero overpotential, $\Delta G_c^{\ddagger}$, were found to range between 5.4 and 5.8 kcal/g-mole. These values are of the same order as presented by Bockris, et al. [7]. The independence of activation energy on substrate indicates a non-binding interaction between the couple and the surfaces (i.e., outer-sphere transfer mechanism).

5.5 Reaction Orders

The values of the anodic and cathodic reaction orders were determined by two methods. In one method [17] the values of the reaction orders were assumed, the theoretical reaction expression was then derived based on these assumptions, and then the experimental data was compared with the theoretical predictions. Figures 5-10 and 5-11 show the experimental data. Table 5-5 shows the comparison of theory with experiment for the assumption that the anodic and cathodic reaction orders are both unity. The close agreement supports the assumed values of unity for the reaction orders. In the second method, a more classical approach was utilized. The reactant concentration under study was varied while maintaining all other concentrations and the potential constant. The variation in the reaction rate with reactant concentration was then measured. The various reactant concentrations employed are shown in Table 5-6 with the results summarized in Table 5-7. As can be seen, the calculated values in many cases deviated significantly from unity.

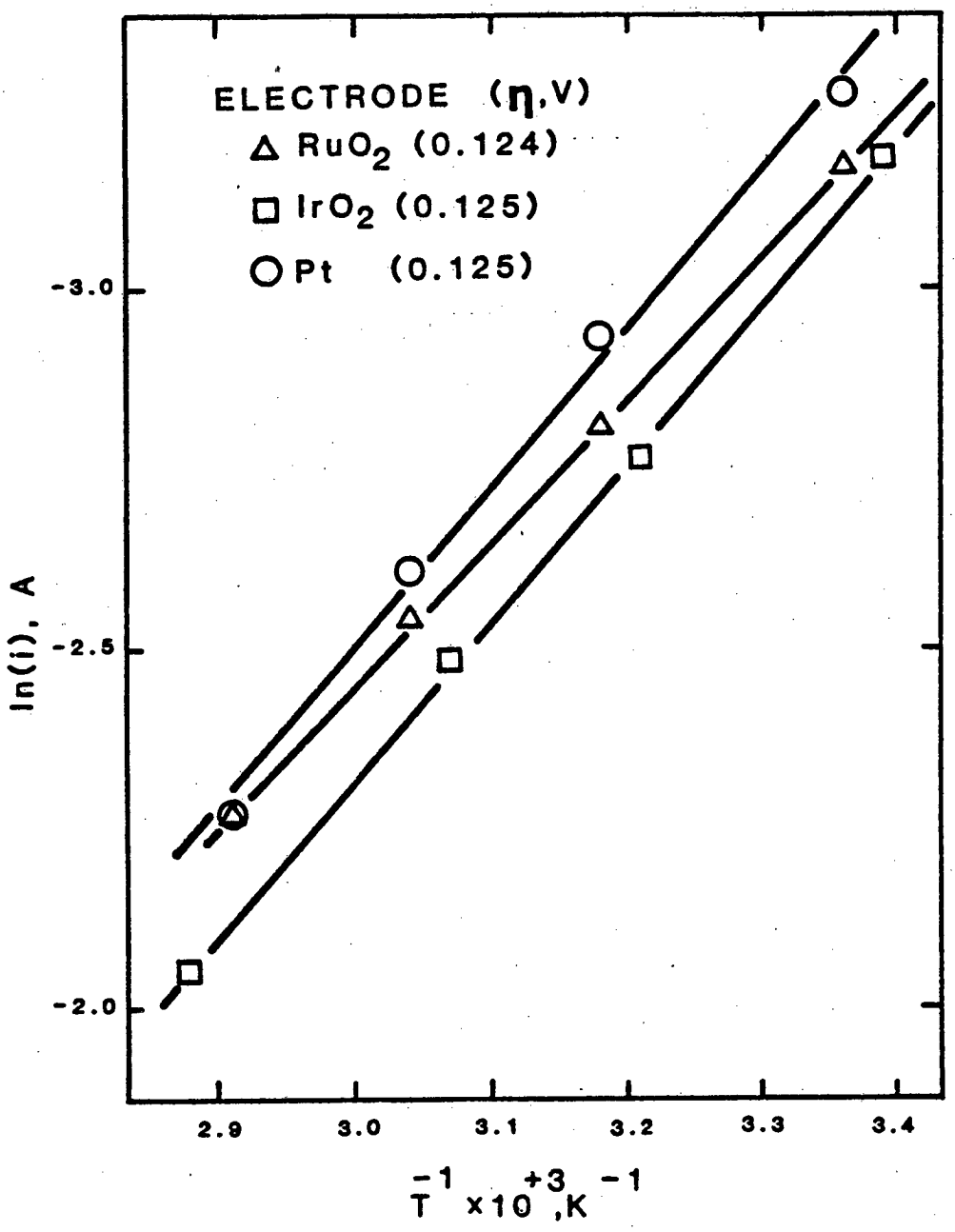

Figure 5-9: Data for calculating free energy of activation of the ferric-ferrous couple at IrO_2, RuO_2, and Pt electrodes.

TABLE 5-4

Free Energies of Activation at Zero Overpotential, $\Delta G_c^{\ddagger}$, for IrO_2, RuO_2, and Pt

Metal	$\Delta G_c^{\ddagger}$(Kcal/g-mole)
Pt	5.76 ± .52
IrO_2	5.80 ± .47
RuO_2	5.40 ± .16

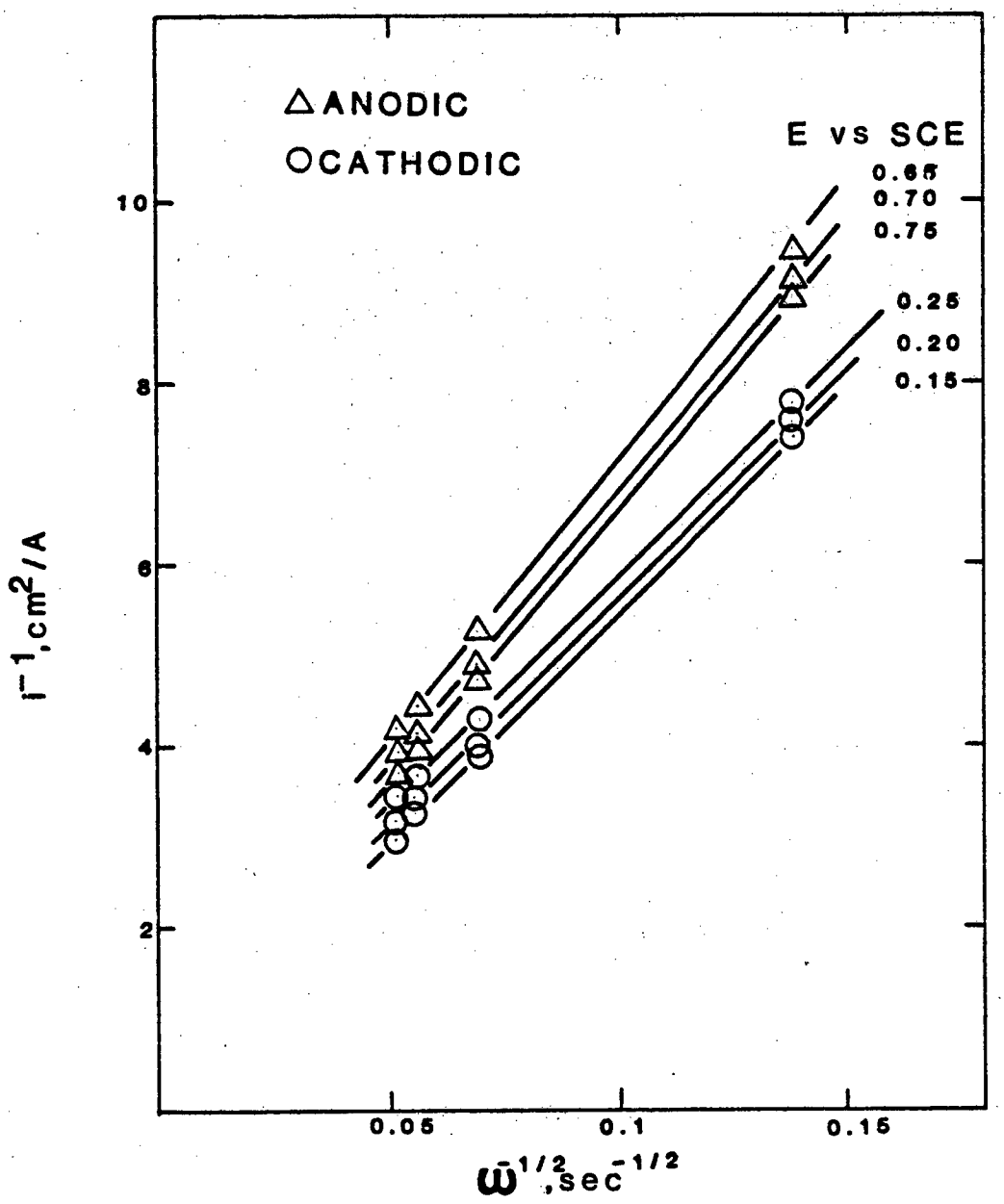

Figure 5-10: Anodic and cathodic reaction order determination for RuO_2 electrodes.

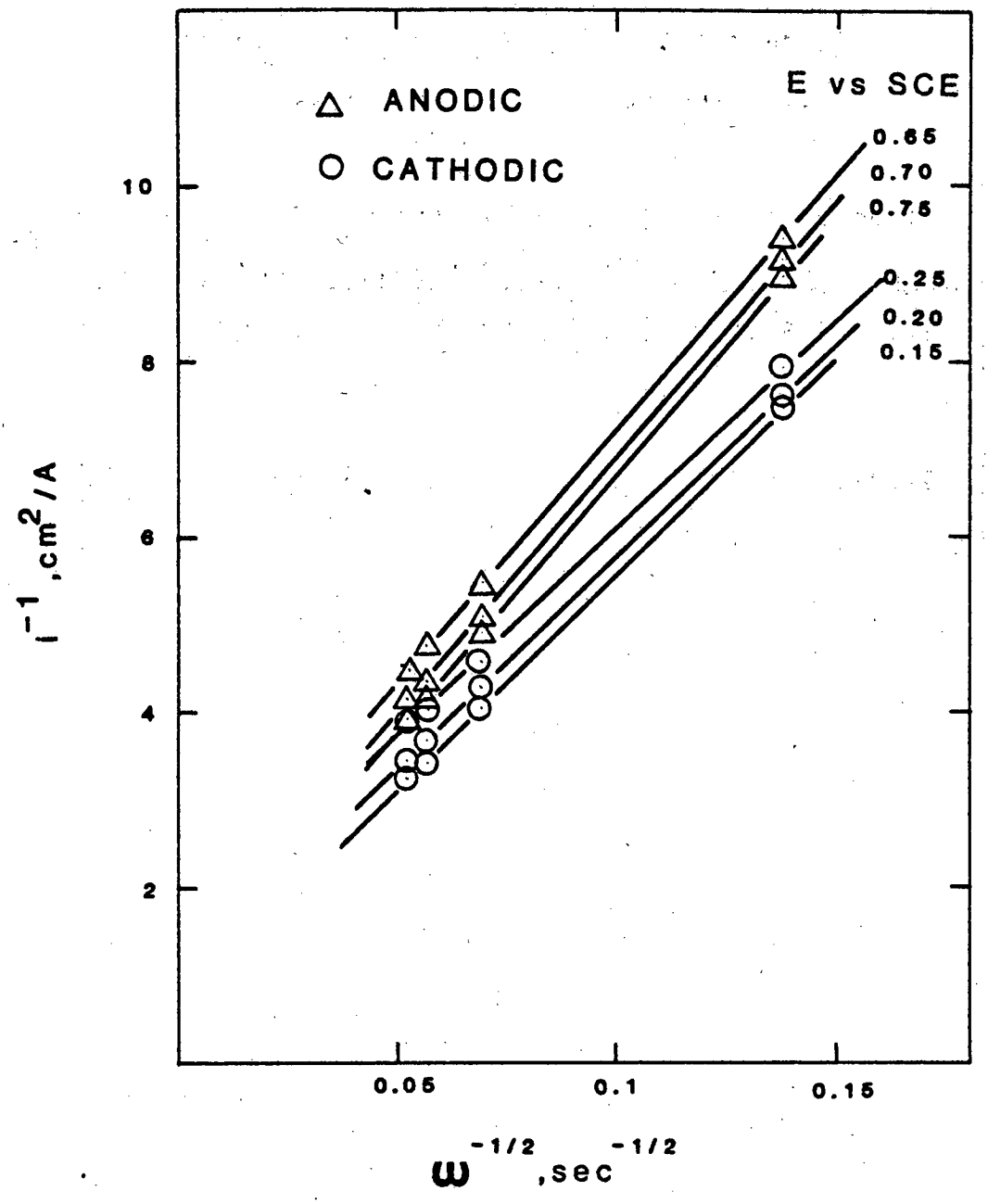

Figure 5-11: Anodic and cathodic reaction order determination for IrO_2 electrodes.

TABLE 5-5

Theoretical and Experimental Values

of B from Equation (22) of Appendix A

Electrode	Theoretical		Experimental		% Difference of Experimental from Theoretical	
	Anodi	Cathodic	Anodic	Cathodic	Anodic	Cathodic
RuO_2 (1-50-1)	61.37	55.62	61.36	50.66	0.02	8.9
IrO_2 (2-10-1)	61.37	55.62	58.30	48.21	5.0	13.3

TABLE 5-6

Variation in Reactant Concentrations (Molarity) and Ionic Strength for Determination of Reaction Orders

	Fe^{3+}	Fe^{3+}	H^+	Cl^-	I
	0.1	0.1	1	1.2	1.75
Cathodic	0.1	0.3	1	1.4	2.75
	0.1	1.0	1	2.1	6.25
	0.1	2.0	1	4.1	16.25
	0.1	0.1	1	1.2	1.75
Anodic	0.3	0.1	1	1.4	2.25
	1.0	0.1	1	2.1	4.00
	3.0	0.1	1	4.1	9.00

TABLE 5-7

Results of Reaction Order Study
Based on Equation (21) of Appendix A
(Variation of Concentration Technqiue)

ELECTRODE SURFACE	ANODIC		CATHODIC	
	E vs SCE	Reaction Order	E vs SCE	Reaction Order
RuO_2	0.7	0.86	0.3	1.04
	0.8	0.77	0.2	0.82
IrO_2	0.7	0.78	0.3	0.73
	0.8	0.78	0.2	0.69

Two explanations can be immediately formulated based on the variation of ionic strength, I, in the above solutions. The ionic strengths are shown in Table 5-6 based on complete dissociation. As can be seen a large variation in ionic strengths is present. A tacit assumption in the calculation of reaction orders by this method is that the potential distribution in the double layer is unaffected by the change in concentration of the species under study. This can be achieved by increasing the supporting electrolyte concentration to maintain I constant. This use of additional acid to compensate for I is probably impractical since the concentration of supporting electrolyte would have to increase to over 15 M in the most severe case. In addition to affecting the double layer potential the change in the ionic strength also has an effect on the activity coefficients of the individual species. The variation in the activity coefficient could thus possibly alter the log current density vs. log concentration plot and thus produce a deviation in the measured reaction order. The above two effects suggest that this method may not be suitable for determination of reaction orders in concentrated solutions.

5.6 Transfer Coefficients

The values of the anodic and cathodic transfer coefficients for RuO_2 and IrO_2 coated RDE's are reported in Table 5-3. This data was calculated by the method of Randles [22] and typical data plots are shown in Figures 5-12 and 5-13. Because the free energy of activation data suggested a simple outer-sphere reaction mechanism, the expected values of the transfer coefficients were 0.5 as predicted by theory [13]. However, the values in Table 5-3 are well below 0.5. In addition, the anodic and cathodic values do not sum to unity as expected. Several tentative explanations for these results were investigated.

At the high concentrations used in these measurements, corrections for the potential drop in the diffuse region of the double layer are usually negligible (especially with specifically adsorbing anions). Therefore, the low values of the transfer coefficients are probably not due solely to double layer effects. The deviation of $\vec{\alpha}$ and $\overleftarrow{\alpha}$ from the theoretical prediction of 0.5 may be due to the following: (1) inapplicability of assumptions used in arriving at a theoretical value for the transfer coefficients; and (2) the dependence of overall $\Delta G^{\ddagger}_{tot}$ on the applied overpotential. The theoretical expression for the free energy of reaction or activation is a sum of various contributions, i.e. work terms, to bring the reactants to and remove the products from the electrode (See Equation (21) in [13]). Of the many assumptions made in arriving at this expression, two pertinent to this discussion are: (1) the electrode is metal; and (2) no specific adsorption or complexing of the reactant occurs. Although single crystals of IrO_2 and RuO_2 possess metallic conductivity, the oxide films of the above metals used in this study had significantly lower conductivities due to nonstoichiometric crystalline structure. Therefore, the properties attributed to metal electrodes may not be applicable to the RuO_2 and IrO_2 electrodes of study. Because $\Delta G^{\ddagger}_{c}$ was found to be

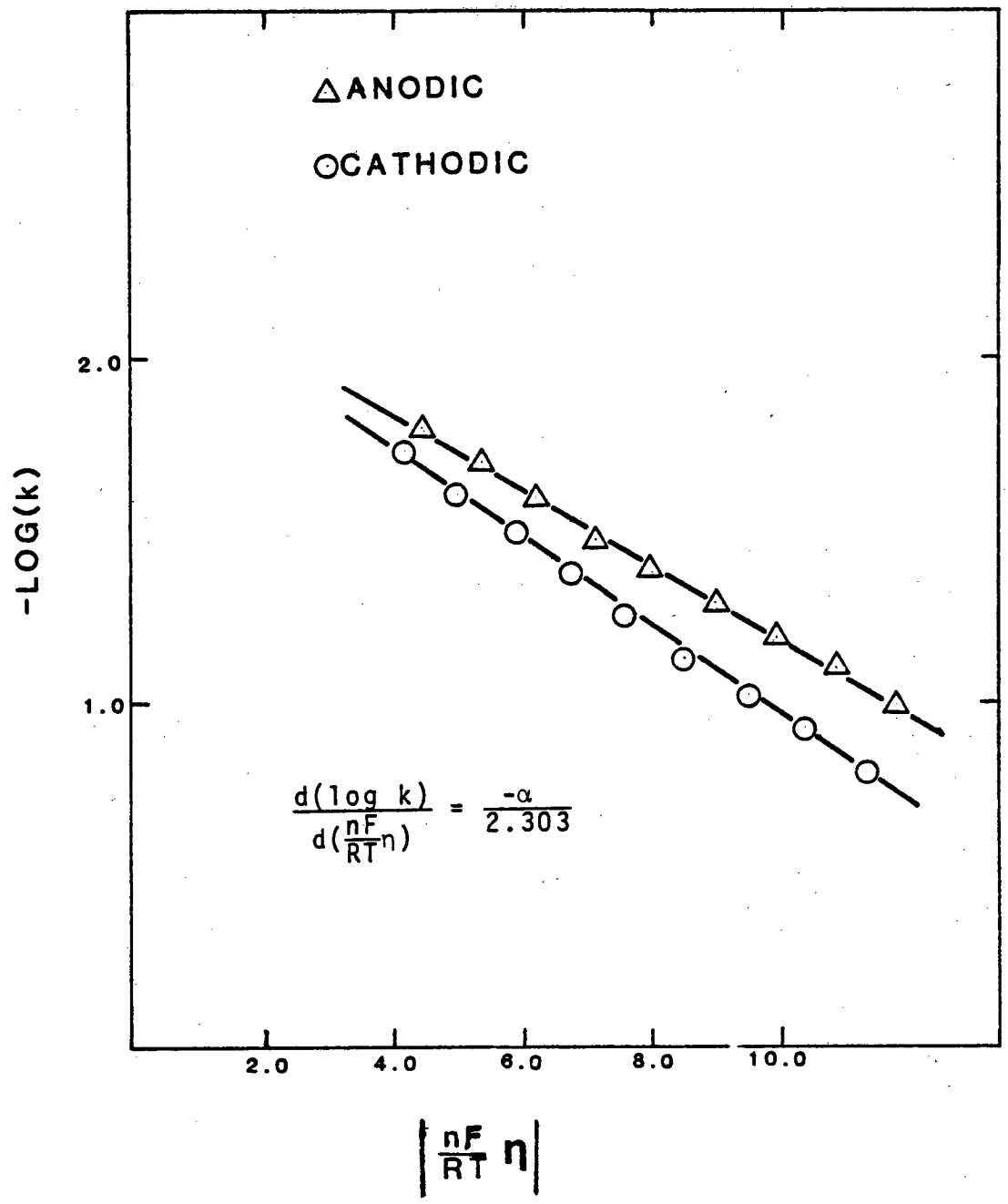

Figure 5-12: Typical plot for determination of anodic and cathodic transfer coefficients for RuO_2 RDE at 3500 RPM.

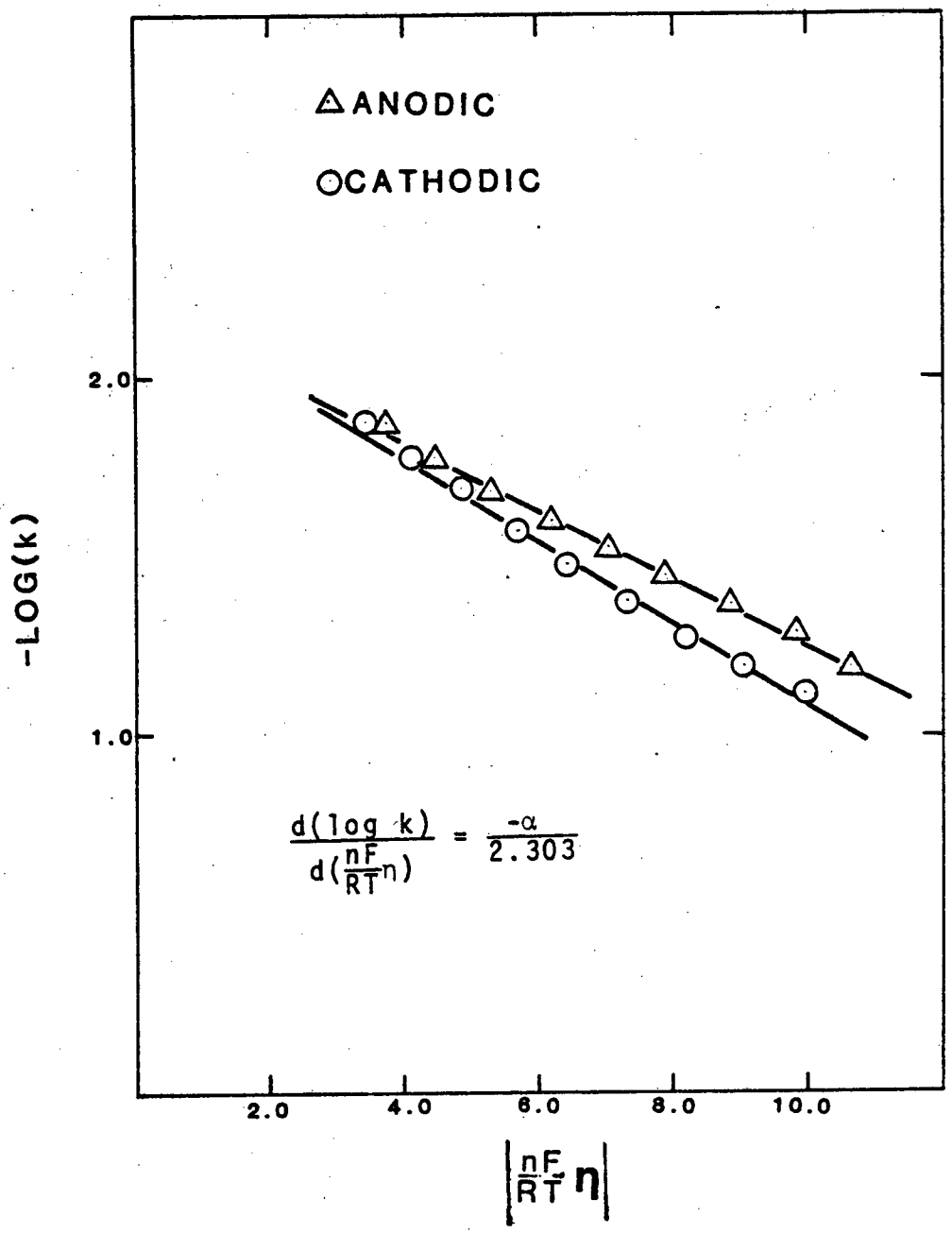

Figure 5-13: Typical plot for determination of anodic and cathodic transfer coefficients for IrO_2 RDE at 3500 RPM.

independent of the substrate employed, little specific adsorption of reactants would be expected. However, complexing of the iron couple with chloride ions is known to occur. Complexing can have a profound effect on the measured value of the transfer coefficient as demonstrated by Gerischer [42]. He found α = 0.4-0.45 for the Fe^{+2}/Fe^{+3} couple at Pt in noncomplexing electrolytes which is in reasonable agreement with the theoretical prediction. However, for the Fe^{+2}/Fe^{+3} couple in the presence of chloride ions, the value of α was 0.2-0.3 at Pt. In addition to the above effects, the overall $\Delta G^{\ddagger}_{tot}$ is dependent on the overpotential (See Equation (29) in Appendix A). For the data used in evaluating $\bar{\alpha}$ and $\bar{\alpha}$, the overpotential changed by approximately 200 mV, thus producing a variation in overall $\Delta G^{\ddagger}_{tot}$ of approximately 2 Kcal/gmole. Since $\Delta G^{\ddagger}_{c}$ is only on the order of 5 kcal/gmole, this variation is appreciable. The consequence of this is a lowering of the slope of the reactant potential energy curve, thus reducing the value of the transfer coefficient [14c]. This argument applies to the measurement of both the anodic and cathodic transfer coefficient. Consequently, the two experimentally measured coefficients should not necessarily be expected to sum to unity [41]. Thus, because of the possible lack of metallic character in RuO_2 and IrO_2 films, the complexing of the reactants, and the dependence of overall $\Delta G^{\ddagger}_{tot}$ on the overpotential, the values of the transfer coefficients can be expected to deviate from the theoretical values. However, additional data is required in order to substantiate the arguments presented here.

6.0 SUMMARY OF RESULTS AND CONCLUSIONS

Knowledge of the true surface area of an electrode surface is necessary in order to compare intrinsic catalytic activity. It was determined that a means of measuring the surface area of a RDE immediately before making kinetic measurements was necessary. The voltammetric charge (0.05 to 1.0 V vs SCE, 20 mV/s, in 1 M H_2SO_4 at 25°C) was used as a means of estimating the disk surface area. The correlation of charge with true surface area (as measured by Zn^{2+} adsorption) has been found using larger electrode samples. For both RuO_2 and IrO_2 coated electrodes, the voltammetric charge and Zn^{2+} measured area were found to have a linear relationship with oxide loading. The correlation for RuO_2 was found to be 6.2 $\pm$ 0.6 Coul/m^2 and for IrO_2 it was 3.5 $\pm$ 0.5 Coul/m^2. The differences in the correlations for the two oxides has been attributed to differences in chlorine content of the two dioxides and consequential differences in grain boundaries and crystal defects.

Low overpotential exchange current densities of the ferric-ferrous couple were measured in concentrated solution (0.5 M Fe^{2+}, 0.5 M Fe^{3+}, 1 M HCl) at Pt, RuO_2 and IrO_2 RDE's. Significant corrections were necessary for ohmic effects, mass transfer effects, and nonuniform current distribution. The data show that the electrocatalytic activity of RuO_2 (k_s = 1.92 x 10^{-3} cm/s) is comparable to that of Pt (k_s = 1.42 x 10^{-3} cm/s) while the activity of IrO_2 (k_s = 1.21x 10^{-4} cm/s) is approximately an order of magnitude less than Pt. Since the measured free energy of activation at zero overpotential was similar for all three substrates (5.4-5.8 Kcal/mole), a non-binding interaction between the couple and the surfaces is suggested (i.e. outer-sphere transfer mechanism). The variation in exchange currents among the different substrates can be attributed to some extent on double layer effects but primarily to crystal structure differences.

The reaction orders of the ferric-ferrous couple in concentrated chloride solutions appear to be first order. However, measured cathodic and anodic transfer coefficients are 0.30 and 0.25 respectively for RuO_2 and 0.26 and 0.20 respectively for IrO_2. The low values of the transfer coefficients as compared to the theoretical predicted values could be a result of the following: (1) inapplicability of assumptions used in arriving at the theoretical value (e.g., metal electrodes, no specific adsorption or complexing of reactants); and (2) significant variation in overall free energy of activation, $\Delta G^{\ddagger}_{tot}$ due to its dependence on the overpotential because of the small values of $\Delta G^{\ddagger}_{c}$, the free energy of activation at zero overpotential.

Regarding the reproducibility of the metal oxide coatings, IrO_2 appears to be more stable than RuO_2. Also, the kinetic data at the IrO_2 surfaces was found to more reproducible. In evaluating porous electrode theory by experiment, a very reproducible electrode surface is desirable so that kinetic rate expressions can be used with confidence. Consequently, it appears as though the IrO_2 coating is a more promising candidate for this application.

APPENDIX A

A. THEORETICAL DETAILS

A.1 Mechanism of Charge Transfer

The theory of charge transfer is essential to an understanding of the reactions occurring at electrified interfaces. An abundance of work remains to be completed in order to develop a complete qualitative and quantitative description of the charge transfer process. The kinetics of electrodic reactions are affected in a profound manner by such elements as the double layer structure, the type of supporting electrolyte, the state of the electrode surface, etc. All of the above interact during charge transfer and separation of the individual effects is usually difficult. Despite these complications, the mechanism of charge transfer can usually be divided into two distinct categories: (1) charge transfer reactions where there is no direct interaction between the reactant and the electrode surface; and (2) reactions involving interaction between the reactant and the electrode surface. In either case, the reactant ion is often hydrated and possibly complexed with a ligand.

A.1.1 Effect of Complexing

For charge transfer reactions in which there is no direct interaction between reactant and electrode, it is generally assumed that the closest approach of the reactant to the electrode surface is the Outer Helmholtz Plane (OHP). These reactions are called simple outer-sphere electron transfer reactions. In dilute solutions of nonadsorbing and or noncomplexing electrolytes (e.g. perchlorate or sulfate media), the ferric-ferrous redox couple has been shown to follow the outer-sphere reaction mechanism [4].

In concentrated solutions, especially chloride medium, complexing between the ferric and ferrous species with chloride ions is known to occur [5]. This means that the solvation sheath surrounding the reacting ions has been altered to a considerable extent such that the electrostatic forces around the ion have also been altered. Consequently, the interaction of this complex with other species in the double layer also could be modified with the result that the complex may be able to move from the OHP to the Inner Helmholtz Plane (IHP). With this increased interaction between the reactant and electrode surface, a definite change in the charge transfer mechansim could be expected. For homogeneous reactions, chloride ion complexed with the ferric and ferrous ions was shown to catalyze the charge transfer reaction [6]. The chloride ion was postulated to lower the energy barrier between the reacting ions caused by the hydration sheaths. In this case, the chloride ion facilitates orientation of the ions for reaction and acts as a bridging agent between the ions during charge transfer.

The above discussion can be extended to the heterogeneous electrochemical reaction system by replacing one of the reactants in solution with an electrode surface. In this situation, the chloride ion may aid the reacting ion in approaching the electrode and thus catalyze the reaction. Galus and Adams [9] and Bockris, et al. [7] have shown that the heterogeneous reaction rate of the ferric-ferrous redox couple was increased in chloride medium over that in sulfate medium. Two possible explanations for the increased reaction rates were postulated by Bockris and coworkers. One explanation involved the chloride ion acting as a bridging agent between the reactant and electrode similar to the homogeneous reaction case. The other explanation was based on the possibility that the reactant concentration in the double layer was appreciably altered by anions in the solution to the extent that the reaction rate was changed.

If ligand bridging is responsible for the enhanced reaction rate in chloride media, then the reaction rate would be dramatically affected by the electrode material employed. This is attributed to the variation in the amount of interaction between the reacting complex and the electrode substrate materials. Consequently, the free energy of activation would be dependent on the electrode material employed. On the other hand, if the observed reaction rate increase was due to concentration effects in the OHP, the electrode material employed would be expected to have only limited effect on the reaction rate because of the limited interaction between the reacting complex and the electrode surface. Therefore, the free energy of activation would be independent of the electrode material. This was observed by Bockris, et al. [7] for the ferric-ferrous redox couple in dilute solutions at Au, Pt, Ir, Rh, and Pd electrodes.

The dependence or independence of the free energy of activation was utilized in this research to determine whether a ligand bridging mechanism or an outer-sphere electron transfer mechanism is applicable in concentrated solutions. In addition to the measurements of the free energy of activation, the values of the anodic and cathodic transfer coefficients were used to test the applicability of a proposed reaction mechanism. According to the theory of electron transfer proposed by Marcus [13], a value of 0.5 for both the anodic and cathodic transfer coefficients is predicted for simple outer-sphere electron transfer reactions. This prediction is supported by experimental data for the ferric-ferrous redox couple in dilute solutions (see Table 2-1). However, experimental data in concentrated solutions are scarce. Thus both the free energy of activation and the transfer coefficients were used to elucidate the mechanism of charge transfer in the concentrated solutions employed in this work.

A.2 Kinetic Rate Expression

The net rate of charge transfer, or reaction rate, is the difference between the anodic and cathodic charge transfer rates. The measure of this net charge transfer rate is the current density, i. It is common practice to assign a positive sign to anodic currents and a negative sign to cathodic currents; this convention was used in this research. The driving force for any electrochemical reaction is the applied electrical potential difference, $\Delta\phi$, commonly referred to as simply the potential. The basic theoretical relationship between the current density and potential is the Butler-Volmer equation. The development of this equation can be found in several texts [14a, 15a] and will not be presented here. Instead, a brief description of this equation will be presented followed by its application in the study of electrochemical reactions.

In general, the overall electrode reaction can be written as

$$O + ne^- = R \qquad (1)$$

Where n is the number of electrons transferred in the overall reaction and O and R represent the oxidized and reduced species, respectively. The Butler-Volmer equation written for the above reaction is

$$i = i_o\left[\exp \frac{\overleftarrow{\alpha} nF}{RT} \eta \; - \exp \frac{-\overrightarrow{\alpha} nF}{RT} \eta \right] \qquad (2)$$

Where i_o is the exchange current density, F is Faraday's constant, R is the gas constant, T is the temperature, $\overleftarrow{\alpha}$ and $\overrightarrow{\alpha}$ are the anodic and cathodic transfer coefficients, respectively, and η is the overpotential. The exchange current density is the rate of charge transfer at the equilibrium potential, $\Delta\phi_e$. Because the electrode-solution interface is in equilibrium at this potential, the anodic and cathodic currents are equal in magnitude but opposite in sign. Thus the magnitude of i_o can be expressed as

$$i_o = nF\overleftarrow{k}_c C_R^P \exp\left(\frac{\overleftarrow{\alpha} nF}{RT} \Delta\phi_e\right) = nF\overrightarrow{k}_c C_o^Q \exp\left(\frac{-\overrightarrow{\alpha} nF}{RT} \Delta\phi_e\right) \qquad (3)$$

where $\overleftarrow{k}_c$ and $\overrightarrow{k}_c$ are the anodic and cathodic chemical reaction rates constants, C_R and C_o are the concentrations of the reduced and oxidized species, and P and Q are the anodic and cathodic reaction orders, respectively. The exchange current density is a measure of the catalytic activity of the particular

electrode-reactant system under investigation. In this research, i_o was utilized to compare the activity of the various transition metal oxides towards the ferric-ferrous redox couple.

The driving force for the reaction is $\Delta\phi$. The applied potential is in fact equal to the sum of the equilibrium potential and the overpotential

$$\Delta\phi = \Delta\phi_e + \eta \tag{4}$$

Rearranging Equation (4) as

$$\eta = \Delta\phi - \Delta\phi_e \tag{5}$$

shows that the overpotential is actually a measure of how far $\Delta\phi$ has deviated from the equilibrium potential. Since the net current is zero at $\Delta\phi_e$, η is the part of the applied potential actually responsible for the production of the net current i.

The form of Equation (2) can be simplified depending on the magnitude of η. The two forms come from the high field and low field approximations. If η is greater than $|0.12|$V then one of the exponential terms, depending on the sign of η, becomes negligible. For example, for anodic polarization (positive value of η) Equation (2) reduces to

$$i \simeq i_o \exp\left(\frac{\overleftarrow{\alpha} nF}{RT}\right)\eta \tag{6}$$

This expression is known as the high field approximation. Taking logarithm of both sides of Equation (6) gives:

$$\ln i \simeq \ln i_o + \frac{\overleftarrow{\alpha} nF}{RT}\eta \tag{7}$$

If i is corrected for mass transfer effects, a plot of ln i vs η should yield a straight line from which the exchange current density (intercept) and the anodic transfer coefficient (slope) can be calculated. The case for cathodic polarization is handled similarly.

In the case of η less than $|0.012|$V, Equation (2) can be linearized by a Taylor series expansion to give:

$$i = (\overleftarrow{\alpha} + \overrightarrow{\alpha}) \frac{i_o nF}{RT} \eta \qquad (8)$$

This expression is known as the low field approximation. It was used for calculating i_o from experimental data in this work (the sum of the transfer coefficients was assumed to be unity).

A.3 Concentration Corrections at the RDE

In this research, the rotating disk electrode (RDE) was used to collect the current-potential data. The RDE was chosen for two reasons: (1) the mass transport of reactants to the electrode can be described by a theoretical solution; and (2) the boundary layer at the electrode surface is stable and reproducible. The basic theory for the rotating disk was developed by Levich in 1942 [16]. Since then, refinements to Levich's development have been made but this has resulted in little change in the basic equations. The complete development and solution of the hydrodynamic flow problem at an RDE can be found in several reviews [17,18] and will not be presented here. Instead only the pertinent equations used in this work will be given.

The current density (anodic or cathodic) at the rotating disk electrode can be written as [15b]

$$i = 0.62nFD^{2/3}\nu^{-1/6}\omega^{1/2}(C_b - C) \qquad (9)$$

where D is the diffusion coefficient of the reactant, ν is the kinetic viscosity of the solution, ω is the angular velocity of the disk, and C_b and C are the reactant concentrations in the bulk solution and at the electrode surface, respectively. The maximum current density occurs when the surface concentration diminishes to zero. At this condition the limiting current-rotation rate relationship becomes:

$$i_L = 0.62\, nFD^{2/3}\nu^{-1/6}\omega^{1/2}C_b \qquad (10)$$

Solving Equation (10) for C_b, substituting into Equation (9) and rearranging yields an expression for the surface concentration of the reactant

$$C = C_b \left(1 - \frac{i}{i_L}\right) \qquad (11)$$

Equation (11) was utilized in this work to eliminate the mass transfer effects permitting the measurement of the reaction parameters under pure kinetic control.

A.4 Corrections for Non-Uniform Current Distributions at the RDE

In the above discussion, a uniform current distribution was assumed to exist at the RDE. The current distribution depends on factors such as homogeneity of the electrode surface, solution resistance, and the kinetic parameters of the reaction under study.

In this study, high exchange current densities are expected due to the use of concentrated solutions and thus the possibility of nonuniform current distribution exists. Failure to account for this nonuniformity can lead to erroneous measurements of kinetic parameters. In this study, corrections for a nonuniform current distribution were made according to Newman [19]. In this method the dimensionless exchange current density, J, is calculated. The definition of J is given as

$$J = (\overleftarrow{\alpha} + \overrightarrow{\alpha}) \frac{nFr_o i_o}{RT\kappa_\infty} \qquad (12)$$

where r_o is the electrode radius, i_o is the apparent exchange current density, and κ is the bulk solution conductivity. With the value of J determined, the ratio of the true to apparent exchange current density can be estimated dpending on the placement of the Lugging capillary tip in relation to the working electrode. The magnitude of the correction as a function of J is reported in graphical form by Newman [19].

A.5 Corrections for Ohmic Drop

Because of the relatively fast reaction rate of the ferric-ferrous redox couple and the use of concentrated working solution, corrections for potential drop in the working solution had to be made. Because of the high currents encountered in the kinetic measurements, a significant potential drop developed in the electrolyte between the working electrode and the reference electrode capillary tip. In this situation, the true overpotential is given by

$$\eta = \Delta\phi - \Delta\phi_e - IR \qquad (13)$$

where I is the total measured current at the controlled potential $\Delta\phi$, and R is the electrolytic resistance. R can be determined by a transient technique described by Newman [20] and McIntyre and Peck [21]. This technique involves measuring the instantaneous potential drop following interruption of the current. In this study, IR corrections were significant, accounting for approximately 40% of the measured overpotential.

A.6 Estimation of Kinetic Parameters

The following discussion deals with the application of the Butler-Volmer equation in conjunction with the theory of RDE in the determination of the electrokinetic parameters.

A.6.1 Transfer Coefficients

Transfer coefficients are useful in elucidating the mechanism of an electrochemical reaction. The anodic and cathodic transfer coefficients are defined as [14b]

$$\overleftarrow{\alpha} \equiv \frac{n-\vec{\gamma}}{\nu'} - r\beta \qquad \text{(anodic)} \qquad (14)$$

$$\vec{\alpha} \equiv \frac{\vec{\gamma}}{\nu'} + r\beta \qquad \text{(cathodic)} \qquad (15)$$

where $\vec{\gamma}$ is the number of electrons transferred in the reaction steps proceeding the rate determining step (RDS), ν' is the number of times the RDS must occur for the overall reaction to occur once, and β is the symmetry factor usually assigned the value 0.5. The factor r is equal to 1 if the RDS is a charge transfer reaction and equal to zero if the RDS is a chemical reaction. The sum of $\overleftarrow{\alpha}$ and $\vec{\alpha}$ is given by:

$$\overleftarrow{\alpha} + \vec{\alpha} = \frac{n}{\nu'} \qquad (16)$$

Equation (16) is useful in testing the consistency of the experimental data. As described previously, the transfer coefficients can be determined by use of the high field approximation. For fast reactions, the electrode response may not pass through a well defined Tafel region and in any event only a fraction of the data is useful with this method.

However, a method proposed by Randles [22] more easily accounts for the corrections for mass transfer effects and the ohmic potential drop. The essential equations employed are:

$$-\log k_c = \log nFC_o^Q \left[\left(\frac{1}{i} - \frac{1}{i_{L,a}} \right) \exp\left(\frac{nF}{RT} \eta \right) - \left(\frac{1}{i} - \frac{1}{i_{L,c}} \right) \right] \quad (17)$$

$$-\log k_a = \log nFC_R^P \left[\left(\frac{1}{i} - \frac{1}{i_{L,a}} \right) - \left(\frac{1}{i} - \frac{1}{i_{L,c}} \right) \exp\left(\frac{-nF}{RT} \eta \right) \right] \quad (18)$$

Equations (17) and (18) are used to determine the anodic and cathodic transfer coefficients, respectively, from the slope of a log k vs $\frac{nF}{RT}\eta$ plot (the slope is $-\alpha/2.303$). In addition, the above equations are applicable whenever the i-η curves can be determined with no restrictions to high or low field approximations. This was the primary method used to calculate $\overleftarrow{\alpha}$ and $\vec{\alpha}$ with the high field approximation used only as a check on the calculations.

A.6.2 Reaction Orders

If the expression for i_o given in Equation (3) is substituted into Equation (2) and $\Delta\phi$ is large enough for the anodic high field approximation to be valid, the result is:

$$i \simeq nF\overleftarrow{k}_c C_R^P \exp\left(\frac{\overleftarrow{\alpha} nF}{RT} \Delta\phi \right) \quad (19)$$

With T and $\Delta\phi$ held constant, the exponential part of Equation (19) is constant. Taking logarithms, of both sides of Equation (19) yields:

$$\ln i \simeq P \ln C_R + \ln(nF\overleftarrow{k}_c) + \frac{\overleftarrow{\alpha} nF}{RT} \Delta\phi \quad (20)$$

Collecting the last two terms Equation (20) into one constant gives:

$$\ln i \simeq P \ln C_R + \text{constant} \qquad (21)$$

If the current is measured at constant $\Delta\phi$ for various concentrations of R, all other concentrations held constant, then the anodic reaction order can be determined from the slope of a ln i vs ln C_R plot. A similar situation exists for the cathodic case.

For an RDE, two simple methods can be employed to calculate the reaction orders [17]. If Equation (21) is used C_R can be replaced by Equation (11). A plot of log i vs log $\left[C_b\left(1-\frac{i}{i_L}\right)\right]$ permits the determination of the anodic or cathodic reaction order from the slope. Alternatively, the value of the reaction order can be assumed and the experimental data tested against this postulation. For example, if P = 1 is assumed, then a plot of i^{-1} vs $\omega^{-1/2}$ should be linear with slope equal to 1/B where

$$B = 0.62\ nFD^{2/3}\nu^{-1/6} \qquad (22)$$

Both methods were used in this study to calculate the anodic and cathodic reaction orders.

A.6.3 Free Energy of Activation

The free energy of activation is not particularly useful in evaluating catalytic activity but it is useful in mechanistic studies. Substituting Equation (4) into Equation (19) assuming anodic polarization and the applicability of the high field approximation yields:

$$i \simeq nF\vec{k}_c C_R^P \exp\left(\frac{\vec{\alpha}nF}{RT}\Delta\phi_e\right) \exp\left(\frac{\vec{\alpha}nF}{RT}\eta\right) \qquad (23)$$

Taking logarithm of both sides of Equation (23) gives:

$$\ln i \simeq \ln \vec{k}_c + \frac{\vec{\alpha}nF}{RT}\eta + \frac{\vec{\alpha}nF}{RT}\Delta\phi_e + \ln (nFC_R^P) \qquad (24)$$

If $\Delta\phi_e$ is replaced by the Nernstian expression

$$\Delta\phi_e = \frac{RT}{nF} \ln \frac{C_o}{C_R} \tag{25}$$

and $\overleftarrow{k}_c$ can be expressed by the activated complex theory [15c] (sometimes referred to as the absolute rate theory)

$$\overleftarrow{k}_c = A \exp\left(\frac{-\Delta G_c^{\ddagger}}{RT}\right) \tag{26}$$

then Equation (24) can be recast as:

$$\ln i = \ln\left[A \exp\left(\frac{-\Delta G_c^{\ddagger}}{RT}\right)\right] + \frac{\overleftarrow{\alpha} nF}{RT} \eta + \overleftarrow{\alpha} \ln \frac{C_o}{C_R} + \ln(nFC_R^P) \tag{27}$$

Rearranging and collecting the temperature independent terms together results in

$$\ln i = \frac{-\Delta G_c^{\ddagger}}{RT} + \frac{\overleftarrow{\alpha} nF}{RT} \eta + \text{constant} \tag{28}$$

or

$$\ln i = \left(\frac{-\Delta G_c^{\ddagger} + \alpha nF\eta}{R}\right) \frac{1}{T} + \text{constant} = \left(\frac{-\Delta G_{tot}^{\ddagger}}{RT}\right) + \text{constant.} \tag{29}$$

Thus the free energy of activation can be determined from the slope of a plot of ln i vs 1/T at constant η.

REFERENCES

1. Ciprios, G., Erskine, W. and P. G. Grimes, "Redox Bulk Energy Storage Systems Study", Final Report NASA Contract No. NAS3-19776, CR-135206, Feb., 1977.

2. L. H. Thaller, "Electrically Rechargeable Redox Flow Cell", U. S. Patent 3,996,064, Dec. 7, 1976.

3. Newman, John and William Tiedemann, "Porous Electrode Theory with Battery Applications", AIChE J. 21, 25 (1975).

4. Schultz, J. W., and M. A. Habib, "Principles of Electrocatalysis and Inhibition by Electrosorbates and Protective Layers", J. Applied Electrochem., 9, 255 (1979).

5. Meites, Louis, Handbook of Analytical Chemistry, (McGraw-Hill N. Y., 1963) p. 1-39.

6. Libby, W. F., "Theory of Electron Exchange Reactions in Aqueous Solutions," J. Phys. Chem., 56, 863 (1952).

7. Bockris, J. O'M., R. J. Mannan, and A. Damjanovic, "Dependence of the Rate of Electrodic Redox Reactions on the Substrate", J. Chem. Phys., 48, 1898 (1968).

8. Angell, D. H., T. Dickinson, "The Kinetics of the Ferrous/Ferric and Ferro/Ferricyanide Reactions at Platinum and Gold Electrodes", J. Electroanal. Chem. and Interfacial Electrochem., 35, 55 (1972).

9. Galus, Z., R. N. Adams, "The Investigation of the Kinetics of Moderately Rapid Electrode Reactions Using Rotating Disk Electrodes", J. Phys. Chem., 67, 866 (1963).

10. Taylor, R. J., A. A. Humffray, "Electrochemical Studies on Glassy Carbon Electrodes", J. Electroanal. Chem. and Interfacial Electrochem., 42, 347 (1973).

11. Miller, R. O., "Electrochemical Kinetic Behavior of 0.2 to 3 Molar Ferrous Chloride-Ferric Chloride Mixtures on Edge-on-Pyrolytic Graphite Rotated Disk Electrodes", NASA TM 73716, July, 1977.

12. Ateya, B. G., L. G. Austin, "The Kinetics of Fe^{+} /FeCl /HCl (aq) on Pyrolytic Graphite Electrodes", J. Electrochem. Soc., 120, 1216 (1973).

13. Marcus, R. A., "Chemical and Electrochemical Electron-Transfer Theory", Ann. Rev. Phys. Chem., 15, 155 (1964).

14. Bockris, J. O'M., A. K. N. Reddy, Modern Electrochemistry, (Plenum Press, N. Y., 1977), Vol. 2, a. pp. 862-892, b. p. 1007, c. pp 922-929.

15. Bard, A. J., L. R. Faulkner, Electrochemical Methods, Fundamentals and Applications, (John Wiley & Sons Inc., N. Y., 1980), a. pp. 86-110, b. p. 290, c. p. 89.

16. Levich, V., Physico-chemical Hydrodynamics, (Prentice Hall, Englewood Cliffs, N. J., 1962).

17. Riddiford, A. C., "The Rotating Disk System" in Advances in Electrochemistry and Electrochemical Engineering, P. Delahay and C. Tobias eds., (Interscience, N. Y., 1966), Vol. 4, pp. 47-116.

18. Opekar, F., P. Beran, "Rotating Disk Electrodes", J. Electroanal. Chem., 69, 1-105 (1976).

19. Newman, J., "The Error in the Measurements of Electrode Kinetics Caused by Nonuniform Ohmic-Potential Drop to a Disk Electrode," J. Electrochem. Soc., 120, 256 (1973).

20. Newman, John, "Ohmic Potential Measured by Interruption Techniques", J. Electrochem. Soc., 117, 507 (1970).

21. McIntyre, J. D. E., Peck, W. F., "An Interruption Technique for Measuring the Uncompensated Resistance of Electrode Reactions under Potentiostatic Control", J. Electrochem. Soc., 117, 747 (1970).

22. Randles, J. E. B., "The Determination of Kinetic Parameters of Redox Reactions from Current-Potential Curves", Canadian J. Chem. 37, 238 (1959).

23. O'Grady, W., C. Iwakora, J. Huang, E. Yeager, "Ruthenium Oxide Catalysts for the Oxygen Electrode", p. 286-297 in Proceedings of the Symposium on Electrocatalysts, M. W. Breiter, ed. (The Electrochemical Society Softbound Symposium Series, Princeton, N. J., 1974).

24. Pourbaix, M., Atlas of Electrochemical Equilibria in Aqueous Solutions; (National Association of Corrosion Engineers, Houston, Tx, 1974), p. 369-370.

25. Weast, R. C., editor, Handbook of Chemistry and Physics, 45th edition, (The Chemical Rubber Company, Cleveland, Ohio, 1964) p. B200.

26. Kozawa, A., "Ion-exchange Adsorption of Zinc and Copper Ions on Silica", J. Inorg. Nucl. Chem., 21, 315-24 (1961).

27. Salkind, A. J., "The Measurement of Surface Area and Porosity", p. 378 in Techniques of Electrochemisty, Vol. 1, E. Yeager and A. J. Salkind, eds., (Wiley-Interscience, New York, 1972).

28. Burke, L. D., O. J. Murphy, "Cyclic Voltammetry as a Technique for Determining the Surface Area of RuO_2 Electrodes", J. Electroanal. Chem., 96, 19-27 (1978).

29. Bishop, E., ed., Indicators (Pergamon Press, New York, 1972), p. 308.

30. Prater, K. B., R. N. Adams, "Critical Evaluation of Practical Rotated Disk Electrodes", Anal. Chem., 38, 153-55 (1966).

31. Bockris, J. O'M. and Srinivasan, Fuel Cells: Their Electrochemistry, (McGraw-Hill, New York, 1969) pp. 496-498.

32. Adams, J. A., "Electrokinetics of the Ferric-Ferrous Couple in Concentrated Solutions at Pt, RuO_2 and IrO_2 Surfaces", M. S. Thesis, University of Akron, Akron, Ohio, 1982 (Available through inter-library loan).

33. Powers, R. W., "A Simplified Preparation of Very High-Purity Water", Electrochemical Technology, 2, 5-6, 163 (1964).

34. Woods, R., "Hydrogen Adsorption on Platinum, Iridium and Rhodium Electrodes at Reduced Temperatures and the Determination of Real Surface Area", J. Electroanal. Chem., 49, 217 (1974).

35. O'Leary, K. J. and T. J. Navin, "Morphology of Dimensionally Stable Anodes", pp. 174-186 in Chlorine Bicentennial Symposium, (The Electrochemical Society, Princeton, N. J.) 1974.

36. Pizzini, S., G. Buzzancz, C. Mari, L. Rossi, S. Torchio, "Preparation, Structure and Electrical Properties of Thick Ruthenium Dioxide Films", Materials Res. Bull., 7, 449 (1972).

37. Newkirk, A. E., D. W. McKee, "Thermal Decomposition of Rhodium, Iridium and Ruthenium Chlorides", J. Catal., 11, 370 (1968).

38. Okamoto, G., T. Shibata, "Stability of Passive Stainless Steel in Relation to the Potential of Passivation Treatment", Corrosion Sci., 10, 371 (1970).

39. Trasatti, S., G. Buzzanca, "Ruthenium Dioxide: A New Interesting Electrode Material. Solid State Structure and Electrochemical Behavior," J. Electroanal. Chem. and Interfacial Electrochem., 29, App. 1-5 (1971).

40. Rogers, D. B., R. D. Shannon, A. W. Sleight, J. L. Gillson, "Crystal Chemistry of Metal Dioxides with Rutile-Related Structure", Inorganic Chem., 8, 841 (1969).

41. Despic, A. R. and J. O'M. Bockris, "Kinetics of the Decomposition and Dissolution of Silver", J. Chem. Phys., 32, 389 (1960).

42. Gerischer, Von H., "Messungen der Austauschstromdichte beim Gleichgewichtspotential an einer Platinelektrode in Fe^{2+}/Fe^{3+} - Losungen", Z. Electrochemie, 54,366 (1950).

43. Burke [28] correlated the charge under the voltammogram with B.E.T. data.

44. It was found that substrate condition, coating technique and electrochemical history all have a marked effect on the resulting true surface area of the electrode.

45. Unpolished titanium substrated but etched in hot concentrated HCl for 2 minutes. Roughness factor based on correlation provided by Burke [28].

TECHNICAL INFORMATION DEPARTMENT
LAWRENCE BERKELEY LABORATORY
UNIVERSITY OF CALIFORNIA
BERKELEY, CALIFORNIA 94720